Master's thesis

NTNU
Norwegian University of Science and Technology
Faculty of Natural Sciences
Department of Physics

Thanh Quyen Nguyen

# A lumped parameters model for cerebral blood flow in neonates and infants with patent ductus arteriosus

Master's thesis in Applied Physics and Mathematics
Supervisor: Rita de Sousa Dias / Hans Torp
June 2019

NTNU
Norwegian University of
Science and Technology

Thanh Quyen Nguyen

# A lumped parameters model for cerebral blood flow in neonates and infants with patent ductus arteriosus

Master's thesis in Applied Physics and Mathematics
Supervisor: Rita de Sousa Dias / Hans Torp
June 2019

Norwegian University of Science and Technology
Faculty of Natural Sciences
Department of Physics

NTNU
Norwegian University of
Science and Technology

*Til min niese Roselin*

# Abstract

A lumped parameters model have been developed to study the dynamics of pulsatile flow in a cardiovascular system (CVS), including the cerebral vascular network. This model was developed from a simplified anatomical configuration and represented by an equivalent electric circuit, where each electric element represents a specific characteristic of the CVS. The aim was to simulate the cerebral blood flow in infants with and without patent ductus arteriosus, a heart condition that affected many infants, especially preterm infants.

In addition to the simulations, cerebral blood flow recordings were also carried out in collaboration with the Neonatal Intensive Care Unit at St. Olavs Hospital. The measurements were performed with Neodoppler, a relatively new ultrasound system developed by Professor Hans Torp and the Ultrasound Group at the Department of circulation and medical imaging, NTNU. These recordings are used both to estimate the model parameters and to validate the results.

Despite a simple approach, the implemented model was able to imitate the typical waveform in both the pressure and flow for the cerebral artery and other segments of the CVS. A series of simulations have also been conducted to assess the connection between the ductus arteriosus (DA) and the distribution of flow and pressure and how they are regulated. The results indicated that the closure of DA involved other regulatory mechanisms in maintaining an optimal level of pressure. The model can be expanded to include these dynamics regulations but was limited by the complexity of the overall effects and limitations of the simulation tool.

# Sammendrag

En lumped parametermodell er utviklet for å studere dynamikken til en pulserende strømning i et sirkulasjonssystem, inkludert det cerebrale vaskulære nettverket. Denne modellen ble utviklet fra en forenklet anatomisk konfigurasjon og representert av en ekvivalent elektrisk krets, hvor hvert elektrisk element representerer en spesifikk egenskap av sirkulasjonssystemet. Målet var å simulere den cerebrale blodstrømmen hos spedbarn med og uten patent ductus arteriosus, en hjertesykdom som rammet mange spedbarn, spesielt premature spedbarn.

I tillegg til simuleringene ble også cerebralt blodstrøm opptak gjennomført i samarbeid med Nyfødtintensiv på St. Olavs Hospital. Målingene ble utført med Neodoppler, et relativt nytt ultralydssystem utviklet av Professor Hans Torp og Ultralydgruppen ved Institutt for sirkulasjon og medisinsk bildediagnostikk, NTNU. Disse opptakene brukes både til å estimere modell parametrene og for å validere resultatene.

Til tross for en enkel tilnærming, var den implementerte modellen i stand til å imitere den typiske bølgeformen i både trykket og strømmen for cerebral arterien og andre segmenter av sirkulasjonssystemet. En serie simuleringer har også blitt utført for å vurdere forbindelsen mellom ductus arteriosus (DA) og distribusjon av blodstrøm og trykk og hvordan de reguleres. Resultatene viste at lukking av DA involvert andre reguleringsmekanismer for å opprettholde et optimalt blodtrykk nivå. Modellen kan utvides til å inkludere disse dynamiske reguleringsmekanismer, men var begrenset av systemets kompleksitet og begrensninger av simuleringsverktøyet.

# Preface

This master thesis is written as part of the five-year master degree programme in applied physics and Mathematics at the Department of Physics in collaboration with Department of Circulation and Medical Imaging at the Norwegian University of Science and Technology (NTNU). It is a continuation of the specialization project from autumn 2018.

I wish to thank Sigrid Dannheim Vik and Martin Leth-Olsen at St. Olav hospital for their support and contributions to collecting NeoDoppler data. I would also like to thank my supervisor Hans Torp who has always been available whenever I need help. His guidance and perspectives on the subject have been really valuable. I want to thank Associate Professor Rita de Sousa Dias for her feedback on the report, which has been helpful. Finally, I would like to thank my research partner Anders Hagen Jarmund who has been a true inspiration. His experience and knowledge have been incredibly useful during development processes.

# Table of Contents

# List of Tables

# List of Figures

# Abbreviations

| | | |
|---|---|---|
| CBF | = | Cerebral blood flow |
| CVS | = | Cardiovascular system |
| CW | = | Continuous Wave |
| DA | = | Ductus arteriosus |
| DBP | = | Diastolic blood pressure |
| GUI | = | Graphical user interface |
| HR | = | Heart rate |
| MAP | = | Mean arterial pressure |
| PDA | = | Patent ductus arteriosus |
| PI | = | Pulsatility index |
| PW | = | Pulsed Wave |
| SBP | = | Systolic blood pressure |
| SV | = | Stroke volume |
| WK-2 | = | Two-element Windkessel model |
| WK-3 | = | Three-element Windkessel model |

Chapter 1

# Introduction

## 1.1 Background and Motivation

Patent ductus arteriosus (PDA) is an abnormal heart condition, where the ductus arteriosus is supposed to be closed right after birth but remaining open. This fetal blood vessel connects the proximal descending aorta to the main pulmonary artery and plays an essential role in the fetal circulation when the lungs are not fully functioning. Infants with an open ductus after birth, typically developed congestive heart failure caused by an increase in blood flow to the lungs (pulmonary overcirculation)[8]. This condition alone accounts for 5-10% of all congenital heart defects [9], where for every 10000 live term births, about 1 to 8 infants are affected by this condition. For preterm infants, the incidence rate can increases to between 25% and 75% depending on their weight and gestational age [10]. Electrocardiography, Chest Radiography, Echocardiography, and Cardiac Catheterization are the main procedures that so far have been used to diagnose and quantify the extent of PDA [11]. However, the effects this condition might induce on the cerebral blood flow are not well-understood. This is mainly due to the lack of measurement techniques to access the cerebral blood flow in infants.

With the development of NeoDoppler, cerebral flow data in infants are now easily accessible. Professor Hans Torp developing this technique at the NTNU Department of Circulation and Medical Imaging in collaboration with NTNU Technology Transfer. The method utilizes the fact that the skull of a newborn baby is not fully developed and there are soft spot areas on the top of the brain called fontanelles, where ultrasound wave can propagate through. By using ultrasound techniques and the NeoDoppler probe, one can sufficiently and thoroughly extract the blood flow information from these areas.

With the development of the NeoDoppler method and a considerable amount of collected cerebral flow data, the need to develop new and more accurate models is essential to increase the understanding of cerebral blood flow.

## 1.2 Literature Review

Chapter 8 in book Heart diseases in children by Khalid Omar M. and co-authors gives a short introduction to the PDA and briefly describes and defines different aspects of the condition, including the rate of incidence, pathology, and pathophysiology. This chapter also mentions briefly some of the main techniques applied to determine the size of DA and to diagnose the disease. It also refers to some clinical scenarios where patients get treated after some examination and symptom observation [11].

Hermes-DeSantis et al. describes in detail some of the mechanisms involving control and regulation of the closure of DA after birth. The clinical findings indicate that prostaglandins (PG) and nitric oxide have an inhibitory effect on the closure of DA. They are endogenous vasodilators produced inside the ductus wall and keep it open by controlling the smooth muscle around the ductus arteriosus. The regulation of these vasodilators and their inhibitors is therefore essential for a more effective closure. In addition to inhibitors, other biological processes under the transitional period, such as energy metabolisms, also influence the constriction of the DA. A typical prostaglandin inhibitor that has been in use since 1970 for the treatment of PDA is the PG Indomethacin [12].

The book Hemodynamics by Mair Zamir explains in great detail the math and physics that define and describe the condition and flow in a vasculature. This book builds on understanding by starting with general equations based on some simple assumptions and then developed into a more and more complicated and realistic scenario. It describes several fundamental concepts and their underlying physics in a very understandable way. The first chapters give a mathematical introduction to some of the properties of a fluid and relevant boundary and input conditions. With a scientific basis in place, Mair Zamir starts to define more specific conditions, starting from a steady flow in a rigid tube to a pulsatile flow and then to pulsatile flow in an elastic tube. Further, the book goes deeper into the topic and discusses more complicated issues, including the effects of wave reflection and the branching of a vascular system. The last part of the book introduces the use of the lumped model to simulate the blood flow in a vasculature. The presented models are simple and based on the similarity between the characteristics of a vascular system and the definition of each electric element. With only four elements in the model, it is only used to describe the relation between the blood flow and pressure [13].

Kokalari et al. wrote a review of methods for modeling the blood flow in systematic arteries, where 40 papers are selected from 250 collected paper regarding the cardiovascular system (CVS) modeling and simulation. This article classifies several categories and methods, ranging from 0D to 3D. The 0D model is one of the simplest forms and is often used in analogy with an electrical circuit. One of the most well-known 0D models is the two elements Windkessel (WK-2) models where a capacitor and a resistance are connected in parallel. This analogy is quite simple but still reflects some important physical properties of the CVS. For more accuracy, more components can be added to the WK-2, typically one or two elements. Experiments indicate that more elements give a better fit with the waveform of flow when compared to the experimental data, especially at higher frequencies. Depends on the objective, more complex representations can be made, by combining sets of elements that either represent one vessel or a specific body part [14].

Tai-Wei et al. review the physiology and pathophysiology of cardiovascular adaptation under the immediate postnatal transitional period. It describes in detail the physiology of fetal circulation and the hemodynamic changes that occurres under preterm births. This article also includes various clinical dilemmas and practical aspects that occur under the transitional period. It also mentions the cerebrovascular autoregulation, which is critical for brain oxygenation and nutrient supply [15].

Garcia-Canadilla et al. developed a computational model of the fetus circulation based on the lumped parameters model concept. The aim was to study the redistribution processes in the cardiovascular systems and how they induce the observed changes in aortic isthmus flow in Intrauterine growth restriction fetuses. This article collects a considerable amount of experimental data regarding the physical properties of central arteries in a systemic circulation system and their anatomical configuration. These physical properties are then used to estimate the values for each element of the model that represents key characteristics related to fetal blood redistribution [1].

## 1.3 Goal and scope

This master thesis aims to develop a computational model of the neonatal circulation to investigate and study the hemodynamic changes under neonatal development. This study was carried out at the same time as the development of NeoDoppler, a relatively new and promising technique and equipment developed to extract cerebral blood flow from newborn infants. The main goal is to assess the feasibility of using a lumped parameters model to simulate flow in a complex vasculature system by pinpointing possibilities and limitations compared to a experimental data. In short, the goals are:

- To understand how a single compartment and its elements of lumped parameters can render the physics and dynamics of real scenarios.
- To develop a computational model of a neonatal circulation, including the cerebral vascular system.
- To assess the possibilities and limitations of the implemented model and development tools.
- To use the model and development tools to simulate dynamically the closure of the DA.

## 1.4 Contributions

This master's thesis is a continuation of the specialization project carried out in the fall semester of 2018. Thus, some of the contents might look similar to the report from that project, especially under the theory and methods sections.

The lumped parameters model developed in this project is based on previous works and concepts collected from literature, especially the one presented by Garcia et al. [1]. These models are then combined and modified to adapt to the neonatal state of infants with a focus on the cerebral blood flow.

The experimental data acquisition from infants is performed by Sigrid Dannheim Vik and Martin Leth-Olsen at St. Olavs Hospital using NeoDoppler and standard Doppler techniques. Professor Hans Torp has developed the ultrasound software and as well as the NeoDoppler probe at the Department of Circulation and Medical Imaging. He has also provided advice and guidance throughout the development of the model.

Previous work by Alex Tran [16] and Anna Wisløff [17], done in earlier semester on the topic of this thesis have also been very inspiring and useful for the writing of this report.

The development process has also been carried out in collaboration with master student Anders Hagen Jarmund who developed a computational model to study the effects of the tilt test on cerebral blood pressure and flow [18]. The basis of our models are similar but elaborated for different clinical scenarios.

## 1.5 Outline of report

This master's thesis contains six main sections. The theory covers all the theoretical aspects related to the subject, including experimental data from the literature. It summarizes the current knowledge on PDA and physical and biological states of a neonatal circulation. Some mathematical descriptions are included to illustrate the underlying physics behind the simulations.

The method section briefly describes the techniques and instruments used in this area, to give an intuitive understanding of the procedure. It also addresses how to use the software and the instruments to acquire and analyze data. The development of the anatomical and electrical model is described in detail under the model development section.

The rest of the sections display the results, discussion, and conclusion, which includes further work.

Chapter 2

# Theory

This chapter covers theoretical aspects of the report that are required to understand the problem, the development process, and to discuss the results. In this report, two aspects have been the main focus: physiological and technical. The physiological aspect defines the problem, while the technical aspect describes the techniques and methods available to solve the problem.

## 2.1 Fetal-neonal Transition

Hemodynamics of the fetal to neonatal transition are orchestrated by a great number of physiological processes responsible for the adaptations required when transferring the respiratory function from the placenta to the lungs. A successful transition typically involves [19] [20]:

- An increased systemic vascular resistance caused by the removal of the placenta. This clinical procedure involves cord clamping that either can happen immediate (ICC) after birth or can be delayed (DCC). The timing and practice varies internationally and is shown to have an impact on the fetal-neonatal transition [21];
- The closure of fetal vascular channels, including the foramen ovale and the ductus arterious. The foramen ovale closes when the left atrial pressure is greater than the right atrial pressure, while the ductus arteriosus reverse its flow within minutes, the closure happens over days;
- A reduced pulmonary resistance caused by an increased oxygen exposure and onset of ventilation; and
- An expansion of the lungs caused by increased respiratory pressure which expands the alveolar air spaces.

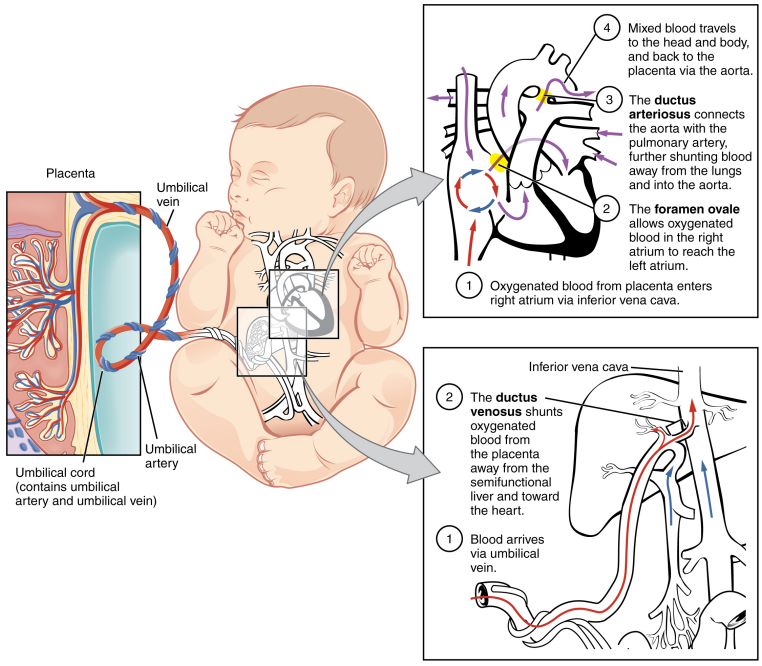


**Figure 2.1:** Diagram of the fetal circulation system. In addition to the ductus arteriosus, the foramen ovale and the ductus venosus also play an important role in the circulation (Wikimedia Commons [4], 2017, licensed under CC BY 3.0 ).

Figure 2.1 illustrates schematically the fetal circulation and shows the location of various fetal vascular channels, including ductus arteriosus, ductus venosus and the foramen ovale. These channels are essential for the fetal circulation to bypass the the pulmonary circulation but close subsequently after birth.

## 2.2 Patent Ductus Arteriosus

The ductus arteriosus (DA) is a vascular structure of the fetal circulation which connects the pulmonary artery and the descending aorta, as shown in figure 2.1. This connection is necessary since it allows deoxygenated blood to be carried from the right ventricle to the placenta where nutrients, gases, and waste products get exchanged. This passage is required since the functionalities of the lungs are not present yet. The oxygenated blood is then carried from the placenta to the right atrium of the heart and bypass the lungs via the foramen ovale to the left atrium [22].

Shortly after birth, the functional closure of DA is initiated. The closure process involves smooth muscle constriction and loss of responsiveness to prostaglandins. Normally, it takes under 48 hours to constrict the ductus and two to three weeks for it to be fully closed (anatomic closure). If the DA is not adequately sealed after 72 hours, the patent

ductus arteriosus (PDA) condition can be diagnosed [12].

Clinical observations in both humans and animals reveal that oxygen tension and circulation level of prostaglandins (PGs) regulate the patency of DA. Low oxygen tension and high level of circulating prostaglandins have shown to keep DA open and functioning. Upon the first breath after birth, the arterial partial pressure of $O_2$ increases leading to an increased metabolism in the lungs, and the dismissal from the placenta decreases the level of prostaglandins. In combination, the overall effect is the constriction of DA. As a result of the constriction, the luminal area of the vessel diminishes and the vessel wall thickened. The wall thickening increases the diffusion pathway for nutrients and gases between the lumen and the outer cells of the vessel, which in turn leads to cell death. In addition, oxygen starvation invokes hypoxic responses, which remodel DA to a fibrous ligament known as the ligamentum arteriosum [12, 10].

In neonates, a persistent PDA with a left to right shunt will cause a redistribution of the systemic blood flow. This reduced systemic blood flow can cause necrotizing enterocolitis (a serious intestinal illness), abnormal cerebral blood flow, and endocarditis (inflammation of the inner lining of the heart). The increased blood flow on the lung side can also lead to overloading and dilation of the left atrium and the left ventricle, where the effect can be heart failure and pulmonary overcirculation [10].

## 2.3 Cardiovascular System

### 2.3.1 The Heart

The human heart is a four-chambers muscular pump consisting of cardiac muscle, the two upper chambers (atria) collect and store blood from tissues of the body and lungs while the two lower chamber (ventricles) pump blood from the heart to the body. The direction of the flow is controlled by four valves, the atrioventricular valves which only allows blood to flow from atria to ventricles and the semilunar valves which ensures on-way flow out of the ventricles [23]. In the fetal and neonatal circulation, the heart also includes the foramen ovale which allows blood to pass between the left and right atrium. The heart pumps its blood by contracting its muscle rhythmically and squirt the blood along. In healthy neonates right after birth, the contraction rate or heart rate (HR) can vary from 68 to 179 beats per minute [24]. The cardiac output (CO) or the amount of blood pumped from the left ventricle per minute is define by the stroke volume (SV) and heart rate, where

$$\mathrm{CO} = \mathrm{SV} \cdot \mathrm{HR} \quad . \tag{2.1}$$

The rhythmic contractions of the heart also generates a pulsatile blood flow throughout the entire vasculature. This pulsatility is characterized by the pulsatility index (PI) [25], where

$$\mathrm{PI} = \frac{\text{Maximum blood flow - Minimum blood flow}}{\text{Average blood flow}} \quad . \tag{2.2}$$

### 2.3.2 Blood Vessel Structures

There are five main classes of blood vessels in a cardiovascular system: arteries, arterioles, capillaries, venules, and veins. The arteries are strong, muscular, and elastic vessels that transport blood from the heart to smaller vessels. The artery walls consist of three layers of different types of tissues: tunica intima (the innermost layer), tunica media (the middle layer) and tunica adventitia (the outermost layer). These layers are made of by connective tissue, elastic fibers, collagen fibers, and smooth muscle cells that give the arteries the elasticity and strength they needed to handle the high pressure exerted by the heart [26].

Arterioles are branches of arteries, with a similar structure but thinner than arterial blood vessels. The arterioles are essential in regulation and control of the blood flow from arteries to capillaries. They provide over 80% of the total resistance to blood flow in the body, and thus the pressure drops significantly over arterioles [27].

Capillaries are the smallest and non-contractile blood vessels in the body. They are typically arranged in networks known as capillary beds. These networks branch from the smallest arterioles and are well integrated with tissues and organs. Capillaries walls are thin and responsible for the exchange of gases, nutrients, and waste between the blood vessels and surrounding tissue [28]. After passing the tissues where exchanges are conducted, the capillaries join and widen to become venules.

Venules convey blood from capillaries to larger blood vessels, namely the veins. Venules have a similar structure as arterioles but are much thinner [29]. The circulation is complete with veins that transport blood from the venules back to the heart. In addition to the three layers found in arteries, veins also have valves which ensure that blood only moves in one direction. The valves are necessary since the pressure in the veins is much lower than the pressure inside the arteries [29]. In addition to valves, skeletal and respiratory muscle pumps also promote the venous return [30]. Another characteristic of the veins and venules is that they are collapsible even under normal condition of pulsatile flow [31].

### 2.3.3 The Arterial Blood Pressure

The arterial blood pressure varies dynamically and requires various parameters to describe its characteristics, including systolic and diastolic blood pressure, pulse pressure, and mean arterial pressure. Clinically, the blood pressure is described as a combination of two values, the systolic blood pressure (SBP) over the diastolic blood pressure (DBP). The systolic blood pressure is the maximum pressure value for each cycle, while the diastolic pressure is the minimum value. The pulse pressure is the pressure difference between the systolic and diastolic values, which describes the pulsatility of the blood pressure. High pulse pressure might indicate high stroke volume or high ejection velocity, while low pulse pressure might indicate high vascular resistance [32]. The mean arterial pressure (MAP) is the steady state component of the pressure waveform. It is an average value estimated for each cardiac cycle and often used to target changes and regulations in a cardiovascular

system. For a given systolic and diastolic pressure, MAP can be estimated by the formula:

$$\mathrm{MAP} = \mathrm{DBP} + \frac{\mathrm{SBP} - \mathrm{DBP}}{3} \quad . \tag{2.3}$$

Figure 2.2 illustrates roughly how the pressure profile and gain develop from the aorta through capillary networks and to the veins. The blood pressure decreases as it moves farther from the aorta due to the vascular resistance and remains low in the venous system. Not only does the pressure changes significantly over the vessels, but also the amount of blood stored in each part. For instantly, only 15% of the total blood volume is stored by the systemic arterial system, while the venous system contains about 75% and the rest 5% circulates in the microvasculatures [30].

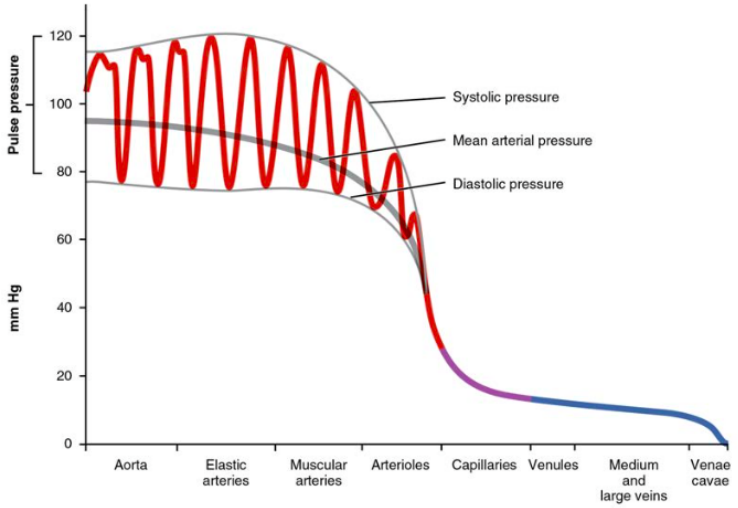


**Figure 2.2:** Arterial blood pressure profile and its components (OpenStax CNX [5], 2016, licensed under CC BY 4.0 ).

### 2.3.4 Blood Pressure, Flow and Resistance Relationship

It is common to adapt the Poiseuille's law to estimate the relation between the pressure and flow for vascular beds, as explained in section 2.4.4. This law defines the vascular resistance as a function of various parameters, including the viscosity of blood, the length, and radius of the vessel. The Poiseuille's approach gives a linear relationship between pressure and flow, which mean that the flow is proportional to the pressure. However under real circumstances, with pulsatile blood pressure and flow in an elastic vessel, this approach is no longer sufficient. Alex Tran [16] and Anna Wisløff [17] did a thorough study regarding pressure-dependent resistance, however the results from these studies did not show a significant difference between pressure-dependent and constant resistance models. In addition, the models in these studies are also simplified for their clinical objectives and do

not focus on the relation between pressure and flow in any specific blood vessel.

reveal the differences between pressure-dependent and constant resistance significantly, but these models are also quite simplified. In addition to the local expansion, blood vessels also have a lower pressure limit or closing pressure, where the vessel collapses if the pressure inside the vessel is lower than the pressure outside [33].

So far, none of the regulatory mechanisms of the blood flow and external conditions have been mentioned. Many mechanisms are involved in blood flow regulation, and it is difficult to simulate or estimate the overall effect. For cerebral blood, the most discussed regulation mechanism is the so-called autoregulation. Autoregulation is important to maintain constant cerebral blood flow for a changing cerebral perfusion pressure. This regulation is essential since the brain is susceptible to pressure and flow changes [34].

## 2.4 Hemodynamics

This section presents some mathematical formulations to describe general states of various systems. Some intermediate calculations will be excluded to promote the overall understanding.

### 2.4.1 Navier-Stokes Equations

In general, the motion of a viscous fluid is described by the Navier-Stokes equations. These equations are derived by Claude-Louis Navier (engineer and physicist) and George Gabriel Stokes (physicist and mathematician) from Newton's second law and the definition of a stress tensor on a fluid element [35, 36]. For a medium with constant density $\rho$, fixed viscosity $\mu$, and no external forces acting on it, these fundamental equations can be expressed in cylindrical polar coordinates by

$$\begin{aligned} \rho\left(\frac{\partial u}{\partial t}+u\frac{\partial u}{\partial x}+v\frac{\partial u}{\partial r}+\frac{w}{r}\frac{\partial u}{\partial \theta}\right)+\frac{\partial p}{\partial x} \\ =\mu\left(\frac{\partial^2 u}{\partial x^2}+\frac{\partial^2 u}{\partial r^2}+\frac{1}{r}\frac{\partial u}{\partial r}+\frac{1}{r^2}\frac{\partial^2 u}{\partial \theta^2}\right) \end{aligned} \tag{2.4}$$

$$\begin{aligned} \rho\left(\frac{\partial v}{\partial t}+u\frac{\partial v}{\partial x}+v\frac{\partial v}{\partial r}+\frac{w}{r}\frac{\partial v}{\partial \theta}-\frac{w^2}{r}\right)+\frac{\partial p}{\partial r} \\ =\mu\left(\frac{\partial^2 v}{\partial x^2}+\frac{\partial^2 v}{\partial r^2}+\frac{1}{r}\frac{\partial v}{\partial r}-\frac{v}{r^2}+\frac{1}{r^2}\frac{\partial^2 v}{\partial \theta^2}-\frac{2}{r^2}\frac{\partial w}{\partial \theta}\right) \end{aligned} \tag{2.5}$$

$$\begin{aligned} \rho\left(\frac{\partial w}{\partial t}+u\frac{\partial w}{\partial x}+v\frac{\partial w}{\partial r}+\frac{w}{r}\frac{\partial w}{\partial \theta}-\frac{vw}{r}\right)+\frac{1}{r}\frac{\partial p}{\partial \theta} \\ =\mu\left(\frac{\partial^2 w}{\partial x^2}+\frac{\partial^2 w}{\partial r^2}+\frac{1}{r}\frac{\partial w}{\partial r}-\frac{w}{r^2}+\frac{1}{r^2}\frac{\partial^2 w}{\partial \theta^2}+\frac{2}{r^2}\frac{\partial v}{\partial \theta}\right) \quad . \end{aligned} \tag{2.6}$$

The velocity components $u$, $v$ and $w$ are velocities of a fluid element in the direction $\hat{x}$, $\hat{r}$ and $\hat{\theta}$, respectively and $p$ is the pressure.

Another fundamental relation that involves the movement of a fluid is the equation of continuity, which can be applied to any conserved quantity. This equation ensures that the total mass is constant over time in a closed system. With the same assumption as above, this relation can be expressed in term of the velocities components.

$$\frac{\partial u}{\partial x} + \frac{\partial v}{\partial r} + \frac{v}{r} + \frac{1}{r}\frac{\partial w}{\partial \theta} = 0 \quad . \tag{2.7}$$

### 2.4.2 Laminar and Turbulent Flow

Osborne Reynolds (British engineer and physicist) observed in 1883 variations in of flow pattern when experimenting with flow in a pipe using dyes. Through a series of experiments, he found that at low velocities the trace elements move in streamlines parallel to each other (laminar), but eventually break down to random motions (turbulence) at higher velocities. In his paper from 1883, he proposed the non-dimensional quantity Reynold number (R), dependent on the velocity and other factors, according to:

$$R = \frac{\rho \bar{u} d}{\mu} \quad , \tag{2.8}$$

where $\rho$ is the fluid density, $\bar{u}$ is the mean velocity, $d$ is the diameter of the tube and $\mu$ is the viscosity coefficient of the fluid. Reynolds experimental data suggest that the transition from laminar to turbulent flow inside a pipe occurs for $R$ between 1900 and 2000 [37, 38].

In a vascular system, the diameters and the velocities for each blood vessel are different. Thus the Reynolds number has a broad range of values in a cardiovascular system. For the human aorta, this value is less than 1000, but since the blood flow is pulsatile and the velocity can sometimes be very high, especially through a narrow passage, this number can be significantly exceeded [39].

The random motions in a turbulent flow are not deterministic and cannot be described by the equations of motion. With turbulent flow, only the mean velocity in the main flow direction can be estimated. In this report, all flows are considered as a laminar flow. This assumption is quite reasonable in most of the cases, especially in healthy infants. However, some conditions can lead to turbulent flow as, for example, the coarctation of the aorta [40].

### 2.4.3 No-slip Condition and Entry Flow

In general, when fluid elements are in contact with a solid surface, it is assumed that the element have no velocity relative to the boundary, this is known as the no-slip condition. For flow in a circular tube, this relation implicates that the first layer of fluid elements is stationary relative to the surface. Further, the velocity in the next layer of fluid will increase progressively towards the center of the tube where it will reach maximum velocity. The slow down effect toward the surface is caused by the viscous resistance between each

liquid layer [39]. The overall effect of viscous resistance is often referred to as vascular resistance.

Consequently, when a uniform flow enters a tube, its entering velocity profile is uniform. As the fluid moves through the tube, the velocity profile changes due to the effect of viscous resistance. Hence the velocities gradually develop a profile where the velocity is at maximum at the center of the tube and decreases continuously toward zero at the surface. After some time, the velocity profile reaches a stabilized state, and its final form is called fully developed. The length required to be fully developed is known as the entry length.

### 2.4.4 Steady Flow in a Tube

A simple approach to assess flow in a vessel is to approximate the vessel to a cylindrical rigid tube with a defined length and radius. Even though this approach is far from reality, since the vessel is elastic and its radius changes periodically as a function of pressure between each cardiac cycle, it is still adequate to evaluate some characteristics of the flow.

From the general Navier-Stokes equations in cylindrical polar coordinates, the system can be more specify by applying or modifying boundaries and states of the system. Starting with a circular boundary condition, all velocity components and the pressure in the tube are independent of the angle $\theta$ and the angular velocity component $w$ will have no amplitude (no rotation). This gives

$$w = \frac{\partial u}{\partial \theta} = \frac{\partial v}{\partial \theta} = \frac{\partial w}{\partial \theta} = 0 \quad , \tag{2.9}$$

which reduced Eq. (2.4) to (2.7) to

$$\rho\left(\frac{\partial u}{\partial t} + u\frac{\partial u}{\partial x} + v\frac{\partial u}{\partial r}\right) + \frac{\partial p}{\partial x} = \mu\left(\frac{\partial^2 u}{\partial x^2} + \frac{\partial^2 u}{\partial r^2} + \frac{1}{r}\frac{\partial u}{\partial r}\right) \tag{2.10}$$

$$\rho\left(\frac{\partial v}{\partial t} + u\frac{\partial v}{\partial x} + v\frac{\partial v}{\partial r}\right) + \frac{\partial p}{\partial r} = \mu\left(\frac{\partial^2 v}{\partial x^2} + \frac{\partial^2 v}{\partial r^2} + \frac{1}{r}\frac{\partial v}{\partial r} - \frac{v}{r^2}\right) \tag{2.11}$$

$$\frac{\partial u}{\partial x} + \frac{\partial v}{\partial r} + \frac{v}{r} = 0 \quad . \tag{2.12}$$

To further simplify these equations, the flow is assumed to be fully developed and the no-slip condition is assumed to apply to the boundary. These new restrictions yield

$$v = \frac{\partial u}{\partial x} = \frac{\partial v}{\partial x} = 0 \quad . \tag{2.13}$$

As a result, Eq.(2.11) is only left with $\frac{\partial p}{\partial r} = 0$, which states that the radial pressure is constant for all radius. The continuity equation (Eq. (2.12)) disappears since all its components are equal to zero and equation 2.10 is further reduced to

$$\rho\frac{\partial u}{\partial t} + \frac{\partial p}{\partial x} = \mu\left(\frac{\partial^2 u}{\partial r^2} + \frac{1}{r}\frac{\partial u}{\partial r}\right) \quad . \tag{2.14}$$

With all these calculations and previous assumptions, the velocity is now only dependent on the radial distance $r$ and time $t$ and the pressure is only dependent on the longitudinal position $x$ and time $t$. To remove the time dependency from the velocity and pressure, the state of the system is assumed to be steady. Under steady state ,the pressure and flow at a specific location will not change as a function of time but remain constant, as given by

$$\frac{\partial p}{\partial x} = \mu \left( \frac{\partial^2 u}{\partial r^2} + \frac{1}{r} \frac{\partial u}{\partial r} \right) \quad . \tag{2.15}$$

From Eq. (2.15), it can be observed that the pressure and flow depend on different variables on each side of the equation. This is only possible if both sides are equal to a constant. Hence Eq. (2.15) can be formulated in term of a constant $k$, where

$$\frac{\partial p}{\partial x} = \mu \left( \frac{\partial^2 u}{\partial r^2} + \frac{1}{r} \frac{\partial u}{\partial r} \right) = k \quad . \tag{2.16}$$

Solving for pressure $p$ and velocity $u$ in relation to the constant $k$ gives

$$p(x) = kx + p_0 \tag{2.17}$$

$$u(r) = \frac{k}{4\mu}(r^2 - a^2) \quad , \tag{2.18}$$

where $p_0$ is the pressure at $x = 0$ (entering pressure) and $a$ is the radius of the tube (for more detail calculation see reference [41]). The resulting expressions (2.17) and (2.18) describes how the pressure and flow developes spatially. With the velocity profile given (Eq.( 2.18)), the flow $q$ can be calculated according to

$$q = \int_0^a u \times 2\pi r dr = -\frac{k\pi a^4}{8\mu} \quad . \tag{2.19}$$

By solving for $k$ using Eq. (2.17) and substitutes with $k$ in equation Eq. (2.19), the relation between the pressure and flow in a tube with length $l$ can be established:

$$q = \int_0^a u \times 2\pi r dr = -\frac{(p(l) - p_0)\pi a^4}{8\mu l} = -\frac{\Delta p \pi a^4}{8\mu l} \quad , \tag{2.20}$$

where $\Delta p$ is the pressure drop between $x = 0$ and $x = l$.

The relation given by Eq. (2.20) is commonly known as Poiseuille flow and is typically expressed in term of a constant $R$

$$\Delta p = Rq, \quad \text{where} \quad R = \frac{8\mu l}{\pi a^4} \quad . \tag{2.21}$$

This constant $R$ (not Reynolds number) quantify the total viscous resistance defined by the system.

### 2.4.5 Pulsatile Flow in Rigid and Elastic Tube

For pulsatile flow as for blood flow, the driving pressure and the resulted flow will vary with time, and Eq. (2.14) will be the one governing the flow and pressure development. The difference in this scenario compared to the Poiseuille flow is that both the pressure and the flow are now dependent on time. In addition to the time dependence, Eq.(2.14) also included a term that describes on the gradient of the radial velocity, $\rho\frac{\partial u}{\partial t}$. This term can be interpreted as an additional resistance which opposes the changes due to pulsatility [42], commonly known as the inertia. If the gradient is small, the flow will remain similar to Poiseuille flow where it simply follows the pressure, but if the changes are rapid, this additional term will cause the flow to lag behind the pressure. Further calculations can be applied to solve the equation, but that is out of the scope of this work.

Further on, to account the fact that blood vessels are elastic and not rigid circular tubes, the current governing equation (Eq. (2.14)) has to be modified. This leads back to Eq. (2.10) to (2.12), where the relations between parameters are much more complicated. Mair Zamir [42] concluded in his analysis regarding the elasticity of a vessel that the most significant difference between a flexible and rigid tube is the occurrence of wave motion. This wave motion involves wave reflection and transmission, which modifies the relationship between pressure and flow at various degrees. The wave reflection is known to arise at every vascular junction, which makes it even more challenging to make a realistic and analytic model.

### 2.4.6 Electrical Analogies

The similarity between vascular systems and electrical systems has been exploited broadly in modeling, simulation, and other fields. The dynamics of pulsatile blood flow can be modeled by utilizing an electric circuit, where its elements are used in analogy with characteristics of a vascular system. From section 2.4.4 one of these characteristics is observed, namely the viscous resistance, where

$$\Delta p = R \times q \quad . \tag{2.22}$$

This relation between pressure and flow describes the viscous resistance ($R$) that opposes the flow in the system. Even though this relation is derived from a steady and fully developed flow for a rigid circular tube, it is still adequate for estimating the total resistance inside a vessel or vasculature. In small vessels and capillaries, the wall elasticity and compliance are small, and hence, the scenario is similar to a rigid tube [14].

In addition to the viscous resistance, the inertia of the system also works as a force that opposes changes of flow and pressure, as described in section 2.4.5. In a cardiovascular system, the driving pressure is pulsatile, which accelerates its fluid elements and also induces an inertial force. For a vessel, it can be shown that the pressure drop due to this resistance is proportional to the gradient of the flow [43]:

$$\Delta p_L = L\frac{dq}{dt} \quad , \tag{2.23}$$

where $L$ is a proportionality constant. In analogy with an electric circuit, this constant is better known as the inductance and is often represented by a coil. For a system with mass $m$ and total force $F$, the inertia relation can be derived from Newton's second law of motion in one dimension ($x$-dimension), where

$$m\frac{d^2x}{dt^2} = F \quad \rightarrow \quad \rho\pi a^2 l\frac{du}{dt} = \Delta p\pi a^2 \quad \rightarrow \quad \rho l\frac{dq}{dt} = \Delta p\pi a^2 \quad . \tag{2.24}$$

Comparing Eq.( 2.24) and (2.23), one can formulate $L$ according to

$$L = \frac{\rho l}{\pi a^2} \quad . \tag{2.25}$$

To account the elastic effect of the vessel wall, a capacitor can be included in the circuit. The non-rigid wall alters its total volume, depending on the pressure. This property defines the compliance of the system. The pressure drop caused by the compliance is described by:

$$\Delta p_C = \frac{1}{C}\int q dt \quad , \tag{2.26}$$

where $C$ is the compliance of the system or a capacitor in analogy with an electric circuit and $q$ is the flow rate that defines the change in volume [43]. With physiological data, the compliance can be estimated for each vessel by

$$C = \frac{3\pi a^3 l}{2Eh} \quad , \tag{2.27}$$

where $a$, $l$, $E$ and $h$ are the radius, length, Young's modulus and thickness of the vessel, respectively [1].

With $R$, $L$, and $C$ defining the functionalities of a vascular system, a complete circuit can be used to model the dynamics of a pulsatile flow, where the pressure is represented by the voltage and the flow is represented by the current in the circuit. The overall analogy and correlation between fluid mechanics systems and electric systems is shown in table 2.1.

**Table 2.1:** Analogous conversion of units between mechanical and electrical properties.

| Mechanical | | Electrical | |
|---|---|---|---|
| Pressure | $\mathrm{mmHg}$ | Voltage | V |
| Flow | $\mathrm{ml/s}$ | Current | A |
| Resistance | $\mathrm{mmHg \cdot s/ml}$ | Resitor | Ω |
| Inertance | $\mathrm{mmHs/ml}$ | Inductor | H |
| Compliance | $\mathrm{ml/mmHg}$ | Capacitor | F |

### 2.4.7 Transient Response

In electrical and mechanical engineering, the transient response is the temporary change in the transition from one state to another, before the system reaches a steady state. Damping oscillation is a typical example of transient response in mechanical systems. In electrical systems, the combination of resistor $R$, inductor $L$ and capacitor $C$ often generates transient oscillations in response to discharges or recharges [44]. For a serial circuit with $R$, $L$, and $C$, it can be shown that the oscillation frequency [45] ($f_{RLC}$) is defined by

$$f_{RLC} = \frac{1}{2\pi}\sqrt{\frac{1}{CL} - \frac{R^2}{4L^2}} \tag{2.28}$$

### 2.4.8 The Lumped Parameters models

The complexity in modeling the relation between pressure and flow in a cardiovascular system is immense, and only simplified approaches have been used to study its dynamics. One of the most common ways to simplify this complex problem is to implement a lumped parameters model. This approach avoids complications by neglecting insignificant details of the system and looking only at the states and properties of the system as a combination of lumped parameters. The vast similarity between the properties of a cardiovascular system and the characteristics of electric elements in a circuit creates the basis for the lumped parameters model in this work. One of the most well-known lumped parameter model for an arterial system is the two-element Windkessel model, introduced by Frank Otto in 1899 [46]. This model describes the pressure-flow relation for an arterial system, using only two parameters, the total peripheral resistance $R_p$ and the total compliance $C$. This model is often illustrated , by analogy, in term of an electric circuit, where a resistor and a capacitor are coupled in parallel, as shown in figure 2.3. The resistor represents the total peripheral resistance and can be estimated precisely by adding up individual resistances in the vasculature or estimated as the ratio between the difference in mean aortic and venous pressure and the cardiac output [6].

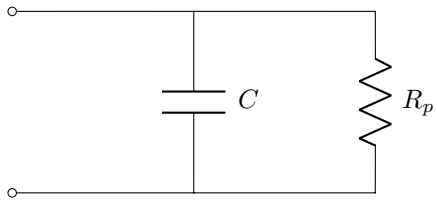


**Figure 2.3:** Electrical representation of the two-element Windkessel model with total peripheral resistance $R_p$ and total compliance $C$.

Similar to the peripheral resistance, the total compliance can also be calculated by adding up the compliance from each vessel. In general, an increment in volume, $\Delta V$, that

results in a variation in pressure, $\Delta P$, gives compliance:

$$C = \frac{\Delta V}{\Delta P} \tag{2.29}$$

For a complex network, the compliance is more difficult to estimate compared to the peripheral resistance since a change in volume will generally result in more than just a change in pressure.

Despite of its simplicity, the Windkessel model was able to predict that the diastolic pressure in the proximal aorta decays as an exponential function. The deficiency of this model was later shown when comparing the results with measured data in the frequency domain, where the WK-2 model fails to comply at high frequency [47]. Figure 2.4 compares the phase and modulus of the impedance for different WK models and the experimental data.

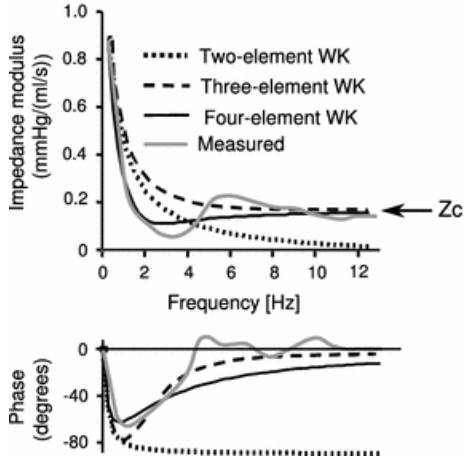


**Figure 2.4:** Measured and simulated aortic input impedance predicted by the Windkessel models(Nico Westerhof [6], 2008, licensed under CC BY 3.0).

The impedance of the WK-2 model decays exponentially and flattens out as it approaches the zero limit, while the impedance in mammals shown a similar decay but tends to a value higher than zero. This value was later found to be equal to the characteristic impedance of the proximal aorta. With this discovery, the WK-2 model was modified by adding a new component, namely the characteristic impedance, coupled in series with the WK-2 model (see figure 2.5). The modified model, WK-3 gives a better fit at high frequencies but also increases the the errors at low frequencies[48]. In this work, the WK-3 model will be utilized to represent the vascular beds.

All the mentioned models so far have been used to represent an entire arterial system. However, these models can also be used to represent one single blood vessel. The representation for each vessel can then be combined into so-called multi-compartments models that represent a network of blood vessels [14]. Many papers have utilized this approach to model cardiovascular systems, where each compartment typically is a combination of

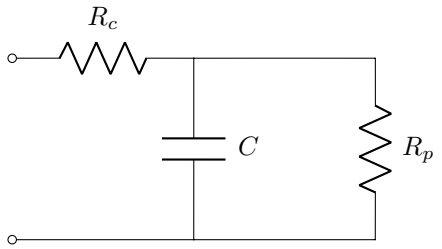


**Figure 2.5:** Electrical representation of the three-element Windkessel model with aortic proximal resistance $R_C$, peripheral resistance $R_p$ and compliance $C$.

three lumped parameters, a resistor, a capacitor, and an inductor [49, 50, 1]. Figure 2.6 illustrates one single compartment and how its lumped parameters are configured. The same configuration is used in the model implemented in this work.

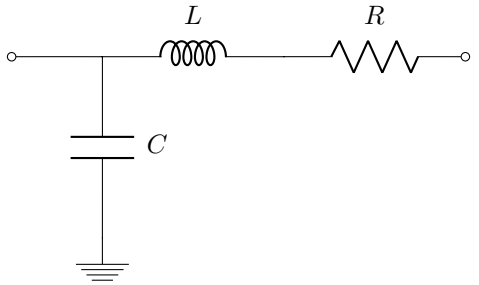


**Figure 2.6:** Single compartment representation of a lumped parameters model, where $R$, $L$ and $C$ represent the viscous resistance,inertance and compliance of a vessel.

## 2.5 Ultrasound Doppler Technique

In this section, a brief introduction is given on the ultrasound techniques and their underlying physics, used to assess the blood velocity and to visualize the interior of a body. Ultrasound technology utilizes the fact that sound waves reflect as they move from one medium to another medium of different density. By recording the time the sound takes to move to a point and back, a point in space can be visualized in form intensity, which depends on the density of the medium at that point. Using scanning techniques, this process can be repeated many times and the data can be combined to create an image. The blood velocity can be accessed using a similar principal by utilizing in addition the Doppler effect. There are two main types of Doppler measurements: Continuous Wave Doppler and Pulsed Wave Doppler, both originate from on the Doppler shift effect. The Doppler shift effect is the change in frequency of a sound received by an observer relative to a moving source. For ultrasonic imaging, the probe is the observer, and the blood is the moving

source. Mathematically, for a fixed probe, the Doppler shift $f_d$ can be expressed by

$$f_d = 2f_0 \frac{vcos(\theta)}{c} \tag{2.30}$$

where $f_0$ is the transmitted frequency, $v$ is the speed of blood components, $c$ is the sound speed for a given medium and $\theta$ is the angle between the direction of the transmitted signal and the direction of the blood. The factor 2 accounts for the two-way transmission, which doubles the shift in this case [51].

### 2.5.1 Continous Wave Doppler Technique

Th continuous wave (CW) doppler technique estimates the speed of blood by continuously sending and receiving ultrasound waves. CW Doppler is commonly done by using one probe with multiple elements where half of the elements are utilized to transmit waves and the rest to receive the reflected waves. These type of measurements are not site specific and the reflector can be anywhere in the overlap region between the two beams. This overlap area can be fairly large, especially if the angle between the beams is small. The received information for a given time is the sum of signals from all scatterers in that region and the observed Doppler shift from these signals is used to estimate the velocity. In term of estimation, a large area will give a small bandwidth for each Doppler shift which makes it easier to distinguish different shifts. On the other hand, information from a large detection area also contain a wider range of values, which makes it difficult to interpreted and since the waves are transmitted and received continuously it is difficult to estimate the location of the signal source [52].

The advantage of this technique is its ability to measure high velocity with good accuracy due to the high sampling rate. Hence, CW Doppler is typically used in cardiac and vascular diagnosis, where a coarctation in a vessel can lead to a rapid increase in velocity.

### 2.5.2 Pulsed-wave Doppler Technique

Pulsed-wave (PW) Doppler, in contrast to CW Doppler, only uses short bursts of ultrasound waves to include the possibility to distinguish the position of the signal. This site-specificity is achieved by transmitting a pulse from a transducer and sampling the received signal after some pre-defined time delay $\tau$. This time delay, also called time of flight (TOF), is calculated from the distance between the scatterers and the probe and taking into account the sound speed in the tissue. For a given distance $z$, the time delay is given as

$$\tau = \frac{2z}{c} \quad , \tag{2.31}$$

assuming that the speed in different tissues are the same. With TOF, the signal can be related back spatially to a location. The size of this location or region of interest $\Delta z$ is related to the pulse duration $T_p$, according to

$$\Delta z = \frac{c}{2} T_p \quad . \tag{2.32}$$

Since the transmission and detection occur sequentially, the same transducer element is used for both transmission and detection. The drawback is that with a short pulse (large bandwidth) it is to difficult to estimate the Doppler shift using only one pulse emission. Instead, sequences of pulses for a given spatial position are used to estimate the velocities of scatterers based on the shift in-depth when a scatterer moves. This phase shift is related to the velocity in a similar manner as the Doppler shift and can be used to estimate the velocity.

Another disadvantage when changing from continuously to sequentially is the limitation of the emission rate. In order to avoid interference, a pulse cannot be transmitted before the signal of the previous one has returned from the point of interest. Hence, the maximum sampling rate or pulse repetition frequency (PRF) is limited by point of interest and the speed in the medium. For a depth, $z$ the $PRF$ is limited by

$$\mathrm{PRF} < \frac{c}{2z} \quad . \tag{2.33}$$

In order to avoid aliasing when sampling the phase shift, the shifted frequency cannot be larger than $PRF/2$, according to the Nyquist theorem , which means that the maximum velocity of scatterers [51] that can be measured on the axial axis is limited by

$$v_{\mathrm{Nyquist}} = \frac{c^2}{8 f_0 z} \quad . \tag{2.34}$$

Chapter 3

# Methods

This chapter describes the techniques and tools used to acquire and analyze Doppler data, especially NeoDoppler. A brief introduction of the simulation tool is also included.

## 3.1 The NeoDoppler Instrument

In collaboration with NTNU Technology Transfer (TTO), Professor Hans Torp has developed a new ultrasound probe that can be attached to the head of newborns to measure the cerebral blood flow continuously. The probe is small and can be placed on top of an open fontanelle where the skull is not fully developed in infants, which made it possible to do ultrasound scanning. This procedure is non-invasive and does not affect the condition of the child or their comfort and therefore can be used continuously to monitor changes in cerebral blood flow. All measured cerebral velocities data in this work were acquired with the NeoDoppler instrument using the Earlybird software. The total setup can be divided into three parts: an ultrasound probe, an ultrasound module and software for processing and display.

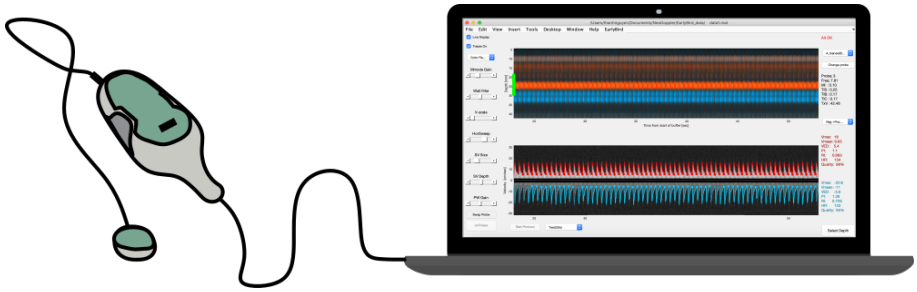

**Figure 3.1:** Illustration of the NeoDoppler device with all its components: a circular probe, an ultrasound scan module and a laptop for analysing.

Figure 3.1 shows a schematic of the components of a NeoDoppler device, showing a circular probe on the left connected to an ultrasound module that controls processing. The data can be processed directly with a laptop or saved for later processing and displaying. In more detail:

- The probe, also known as the transducer, has only a single element which both sends and receives sound waves. It is circular with a diameter of 1-2 cm. The transducer surface is flat, which means that it is geometrically unfocused. The transducer is made such that it can process information down to a distance 1-2 times the diameter of the probe.
- The scanner module consists of electronic components, that generates pulse-wave for transmission and preprocesses wave signals on received.
- A laptop or other graphical user interface is used for further processing and displaying. The Earlybird software is specifically developed for this purpose. This software can be used as a user interface for real-time observation or for analyzing the saved data.

## 3.2 EarlyBird Software

For the purpose of processing and extracting physiological information from the measurements, the EarlyBird Software was developed. It is a collection of packages and Matlab scripts for analyzing and displaying measured cerebral blood velocity. The codes are written in Matlab language and can therefore only run on Matlab platform. The program contains a graphical user interface that can run on both real-time, by connecting to a scanner, or offline by loading saved data. While clinicians use the program in real-time to do measurements and collect data, this report will only focus on how to load and run calculation on saved data.

The offline modus of the program can be activated by running a specific Matlab script. At launch, a graphical user interface (GUI) will appear. From here saved data can be

loaded using the load data option under the module Earlybird. The data can be chosen from any folder but have to be of type mat-file. When the loading is done, the GUI will show two graphical windows as shown in figure 3.2.

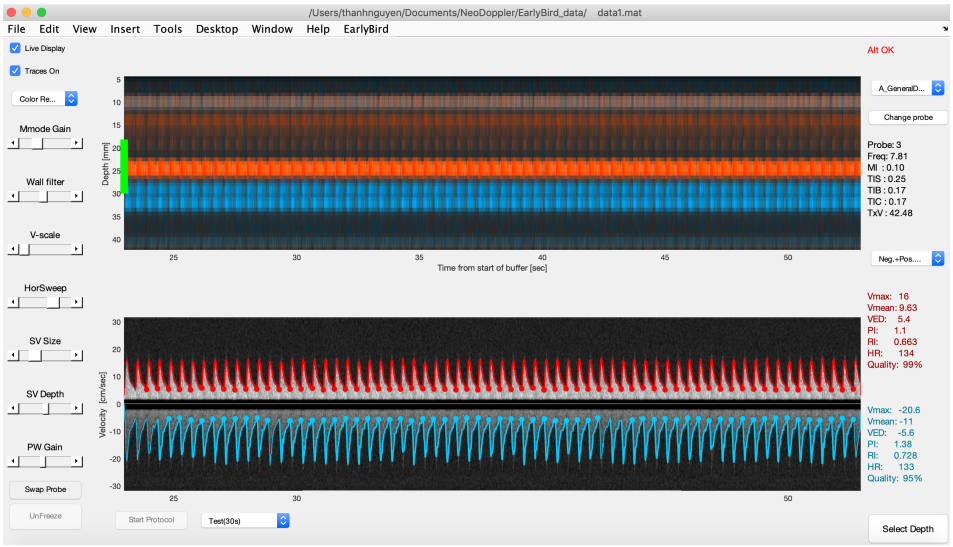


**Figure 3.2:** Graphical user interface for the EarlyBird sofware.

The upper window of the GUI displays the intensity of signals there is at each layer or depth and how it varies with time. The color indicates the direction of the flow and the intensity shows the strength of the signal at a particular location and time. The green bar shows the data interval that is selected for display in the lower window. This bar is controlled by the options on the left side of the GUI. The positive and negative blood velocity as a function of time is shown in the lower window. In addition to options to change the region of interest, the left side of the GUI also contains other options to reduced noise or increase blood signal. On the right side of the GUI, various estimated values can be found such as maximum/minimum speed, pulsatile index (PI), and so on. These values are estimated from the waveforms in the lower window. In order to analyze or apply more calculation on the velocity, the point data is required. This is done using the *getvelocitytracer*-script

## 3.3 Physiological Recordings

Clinical recordings of infants were performed at St. Olav's hospital in Trondheim with consent from their parents by hospital personnel. Cerebral blood velocity is acquired by NeoDoppler as described in section 3.1, and blood velocities at other locations were measured with standard Doppler techniques and probes. Measurements on infants with PDA were performed by Martin Leth-Olsen, while measurements on normal infants were per-

formed by Sigrid Dannheim Vik, both from The Department of Circulation and Medical Imaging.

The cerebral blood velocity is measured through the frontal fontanelle on the top the head of newborns. The skull in this area is not fully developed and allows acoustic transmission. In order to monitor the change in velocity continuously, the transducer is connected to the head with a fastening device, a hat in this case. A typical cerebral waveform is shown in figure 3.3 for healthy an infant.

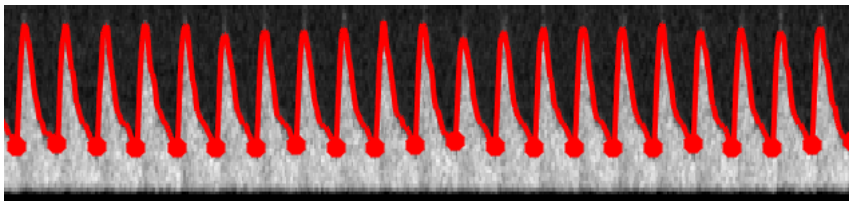

**Figure 3.3:** NeoDoppler spectrum for a healthy infant presented by the Earlybird software.

The physical and clinical condition of the infants are not relevant perspectives for this work, except for infants with PDA, and the data is only used as a quality check and for the purpose of estimation and analysis of the information stored within each cycle. The physical condition and various regulation mechanisms will affect the values of measured data. In the model, the parameters are estimated such that the model-based results fit with the measured values in a steady state condition. Hence the change in these estimated parameters can be used to reflect what kind of condition or state the patient has if enough data is collected.

So far only one set of the measurements for one infant with significant PDA diagnosis is available and hence this set is only used qualitatively to compare with simulated results.

## 3.4 The Simscape Simulation Tool

There are many simulation tools available to simulate hemodynamics of a cardiovascular system, especially as an electric circuit. For simplicity, flexibility, and accessibility, Simscape is chosen as the main simulation tool in this work. Simscape is a simulation package, extended from the well-known Simulink package developed by Mathwork. It is a block-based diagram environment for Model-Based design [53]. Simscape can be used for several purposes including simulation of physical, mechanical and electrical systems. The developed model is an anatomically analogous circuit and will therefore use the electric part of the program.

Simscape (Simulink) is integrated with Matlab, but it also has its own GUI where different systems can be implemented. A system can simply be implemented by using components from the Simulink and Simscape library utilizing the drag and drop principles. The program allows the user to make their own components using the Matlab workspace or by

combining existing components in the library. All simulations can be conducted directly from the Simscape GUI, where the results can be visualized using the scope component or indirectly using Matlab, where more advanced options are available. Using Matlab as the control unit gives many advantages, including better control of the simulation and more flexibility in the extraction and analyses of the results.

In Simscape, simulations are controlled by a global solver which provides a range of options and tools. Some of the main options used in this work are listed in table 3.1.

**Table 3.1:** Global solver configuration for Simscape simulation.

| | |
|---|---|
| Type : | Variable-step |
| Solver : | od23t (mod. stiff/Trapezoidal) |
| Max step size : | auto |
| Min step size : | 1e-7 |
| Relative tolerance : | 0.01 |
| Absolute tolerance : | auto |

Chapter 4

# Model Development

The model developed in this work is based on the previous work done by Garcia et al. [1] and many others [54, 49, 50, 14]. The theory behind all these models can be traced back as early as 1899 by Frank Otto[46], but the methods have became more and more advanced and the models are more complex and accurate. The implemented model is mainly derived from Garcia computational model, mostly by using the collected experimental data regarding the configuration and physical dimension and properties of each blood vessel. Garcia computational model was developed in analogy to fetus anatomy with some simplification and an intention to investigate the blood flow change in Intrauterine growth restriction (IUGR) fetuses.

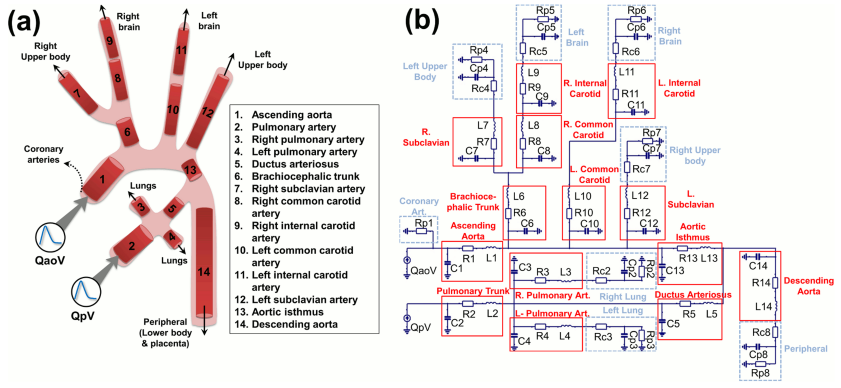


**Figure 4.1:** Illustration of an anatomical simplified configuration and its equivalent lumped parameters model for a fetal circulation (Garcia-Canadilla et al [1], 2014, licensed under CC by 3.0 )

Figure 4.1 shows an illustration of a simplified configuration of a fetal circulation on the left and its corresponding lumped model on the right as presented by Carcia et al [1].

Each central blood vessel or a section of a central blood vessel is represented by a block of three electric elements, a resistor $R$, an inductor $L$ and a capacitor $C$, which correspond to the resistance, inertance and compliance, respectively , in a blood vessel. Smaller blood vessels and capillaries are integrated into one single block also with three elements and can either represents a network of blood vessels in one single organ or organs. The values of each parameters central artery are calculated from experimental data, while the rest are estimated such that the flow and its distribution fit with the observations.

In this work, the proposed model is a modification and adaptation from previous models by adding more blocks and complexity to simulate the cerebral blood flow in infants. The purpose is to investigate the applicability of electrical components in a complete electric circuit as a lumped parameters model to simulate the cerebral blood flow. The complexity of the structure and the functionalities of the real scenario are greatly simplified and represented by a combination of electric elements, similar to the approach taken by Garcia. The functionality of each vessel and their network are described by the characteristics of the elements in each compartment and how they are combined. Nearly all biological processes and regulatory mechanisms are excluded from the implemented model due to the complexity and the uncertainty of their effects. However, some mechanisms can be included by adding more components or functionalities to the model or the simulation tool. With this setup, it is possible to some extent to investigate the overall pressure-flow relationships and the flow distribution at various locations under some predefined conditions. The increased number of compartments in this model compared previous ones[1, 54] gives an advantage in following the flow and its change along the vessel, since more compartments are available for each vessel. Another important aspect, that might affect the waveform significantly is the wave response (transmission and reflection) caused by the elasticity of the wall and the pulsatile flow, which is not included in this report [42]. In addition to internal effects, external phenomena like gravity and the state of the patient (standing, sleep, scared ...) also affect the measured flow and pressure. The impact from these external phenomena might have an overlapping effect with the internal regulations and these are assumed to only affect the values of the model parameters and not the configuration of the system.

## 4.1 The Anatomical Configuration

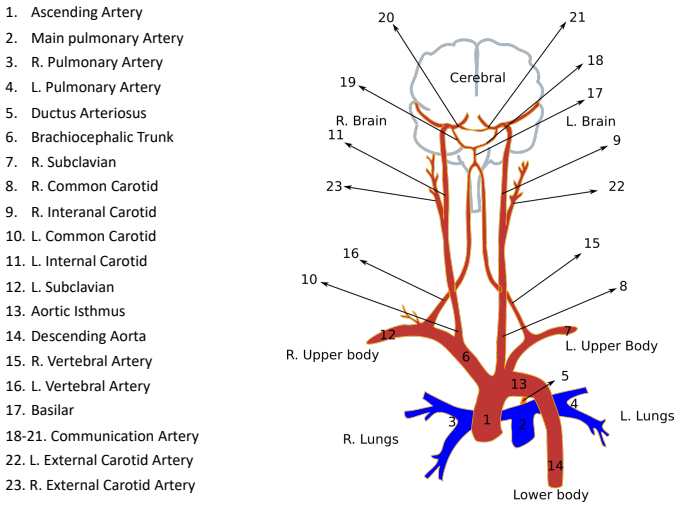


**Figure 4.2:** A simplify anatomical illustration of the neonatal cardiovascular system. The red and blue part represent the systemic and pulmonary circulation, respectively. The ductus arteriosus is open and creates a connection between the ascending artery and main pulmonary artery.

Figure 4.2 shows a simplify neonatal circulation with 23 main arterial segments, including the ductus arteriosus. The systemic circulation is shown in red, excluding all parts that are not connected directly to the brain. The pulmonary circulation is shown in blue and is connected to the systemic circulation via the ductus arteriosus. This anatomical model also includes a complete Willis circle in the brain, which regulates and distributes the flow to every part of the brain. However, this circle varies a lot in structure from infant to infant [55]. Another importance simplification that is shown in the figure but not included in the model is the left and right external carotid (22,23) that deliver blood to the face. These arteries are not included due to the increased complexity of the system which increases the instability of the simulation. Without these arteries, the amount of blood to the brain is expected to be higher. In addition, the developed model does not included a heart or a vein system due to their complexity. Excluding the heart does not change the outcome as long as the input flow to the system accounts all effect from the heart. The effects from vein system are also trivial, since its pressure and flow is low compared to the arterial side.

To simulate flow and its distribution in a circulation system, it is not enough to just have knowledge on the configuration, but information on the the physiological data regarding the system is also needed. This includes the physical dimension and properties of each blood vessel. Such data can be found in previous papers [1], but refer to fetus circulation and not neonatal circulation. Hence the data is used assuming that these values do not change significantly on the transition from fetus to newborn. Data , concerning the cerebral network, is estimated based on adult values and scaled to fit the data on fetuses [2].

In the model developed in this work, the cerebral network is included to specifically simulate the blood flow at the anterior cerebral, which is more compatible to compare to the NeoDoppler measurements that capture signals through a fontanelle. It consists of right and left vertebral artery, basilar and communication arteries. Table 4.1 listed all the values and how they are related to the gestational age in form of equations. Beside the properties of the blood vessels, also properties of the fluid, such as the density $\rho$ and viscosity $\mu$ play an important role in the description and validity of the model, where $\mu = 2.5\mathrm{cps}$ [56] and $\rho = 1.05\mathrm{g/cm}^{-3}$ were used.

**Table 4.1:** Physiological properties of central arteries as functions of gestational age (GA), including length, radius and Young's modulus (E) of the vessel. These relations are partly presented by Garcia, et al [1] and the rest are estimated by comparing to adults values [2]

| Vessel | length (mm) | diameter (mm) | E($\mathrm{dyn/cm}^2$) |
|---|---|---|---|
| Ascending Artery | $-8.61 + 0.88{*}$GA | $-2.10 + 0.27{*}$GA | $7.5 \cdot 10^5$ |
| Main pulmonary Artery | $-5.60 + 0.57{*}$GA | $-2.77 + 0.30{*}$GA | $7.5 \cdot 10^5$ |
| R. Pulmonary Artery | $-4.00 + 0.41{*}$GA | $-1.71 + 0.18{*}$GA | $7.5 \cdot 10^5$ |
| L. Pulmonary Artery | $-4.00 + 0.41{*}$GA | $-1.95 + 0.19{*}$GA | $7.5 \cdot 10^5$ |
| Ductus Arteriosus | $-2.41 + 0.31{*}$GA | $-2.09 + 0.21{*}$GA | $13.5 \cdot 10^5$ |
| Brachiocephalic Trunk | $-1.056 + 0.29{*}$GA | $-1.78 + 0.18{*}$GA | $7.5 \cdot 10^5$ |
| R. Subclavian | $-2.15 + 0.43{*}$GA | $-1.22 + 0.12{*}$GA | $9.0 \cdot 10^5$ |
| R. Common Carotid | $-8.25 + 1.36{*}$GA | $-1.52 + 0.14{*}$GA | $9.0 \cdot 10^5$ |
| R. Interanal Carotid | $-8.25 + 1.36{*}$GA | $-1.22 + 0.11{*}$GA | $13.5 \cdot 10^5$ |
| L. Common Carotid | $-9.69 + 1.59{*}$GA | $-1.52 + 0.14{*}$GA | $9.0 \cdot 10^5$ |
| L. Internal Carotid | $-8.25 + 1.36{*}$GA | $-1.22 + 0.11{*}$GA | $13.5 \cdot 10^5$ |
| L. Subclavian | $-2.15 + 0.43{*}$GA | $-1.22 + 0.12{*}$GA | $9.0 \cdot 10^5$ |
| Aortic Isthmus | $-2.15 + 0.22{*}$GA | $-1.86 + 0.19{*}$GA | $7.5 \cdot 10^5$ |
| Descending Aorta | $-34.25 + 3.57{*}$GA | $-2.22 + 0.22{*}$GA | $9.0 \cdot 10^5$ |
| R. Vertebral Artery | $-6.68 + 1.10{*}$GA | $-0.83 + 0.08{*}$GA | $13.5 \cdot 10^5$ |
| L. Vertebral Artery | $-6.68 + 1.10{*}$GA | $-0.83 + 0.08$GA | $13.5 \cdot 10^5$ |
| Basilar | $-1.32 + 0.22{*}$GA | $-1.00 + 0.09{*}$GA | $18 \cdot 10^5$ |
| Communication Artery | $-0.70 + 0.12{*}$GA | $-0.45 + 0.04{*}$GA | $18 \cdot 10^5$ |

## 4.2 The Simscape Model

From the anatomical model shown in figure 4.2, excluding the left and right external carotid arteries, an electrical lumped parameter model was constructed. This is based on the analogy between a physiological system and an electric circuit. The entire vascular network is replaced by an electric network with a similar configuration, where blood flow and pressure are represented by current and voltage, respectively. The characteristic of each blood vessel and their impact on the flow and pressure are now controlled by properties of various electric components. The resistance to flow cause by the viscosity of blood in interaction with the wall is represented by a resistor, coupled in series to the

path. The inertance that impedes the change in the flow is controlled by an inductor and the way a pressure change affects the blood vessel volume is regulated by a capacitor (see section 2.4.6). Figure 4.3 shows the overall configuration of the system. It consists of flows sources (on the top) that represent the flows that come out of ventricles and into the system, central arteries are visualized by boxes with various colors (see below for more details) and the vascular beds are simplify and represent by light blue blocks of three components.

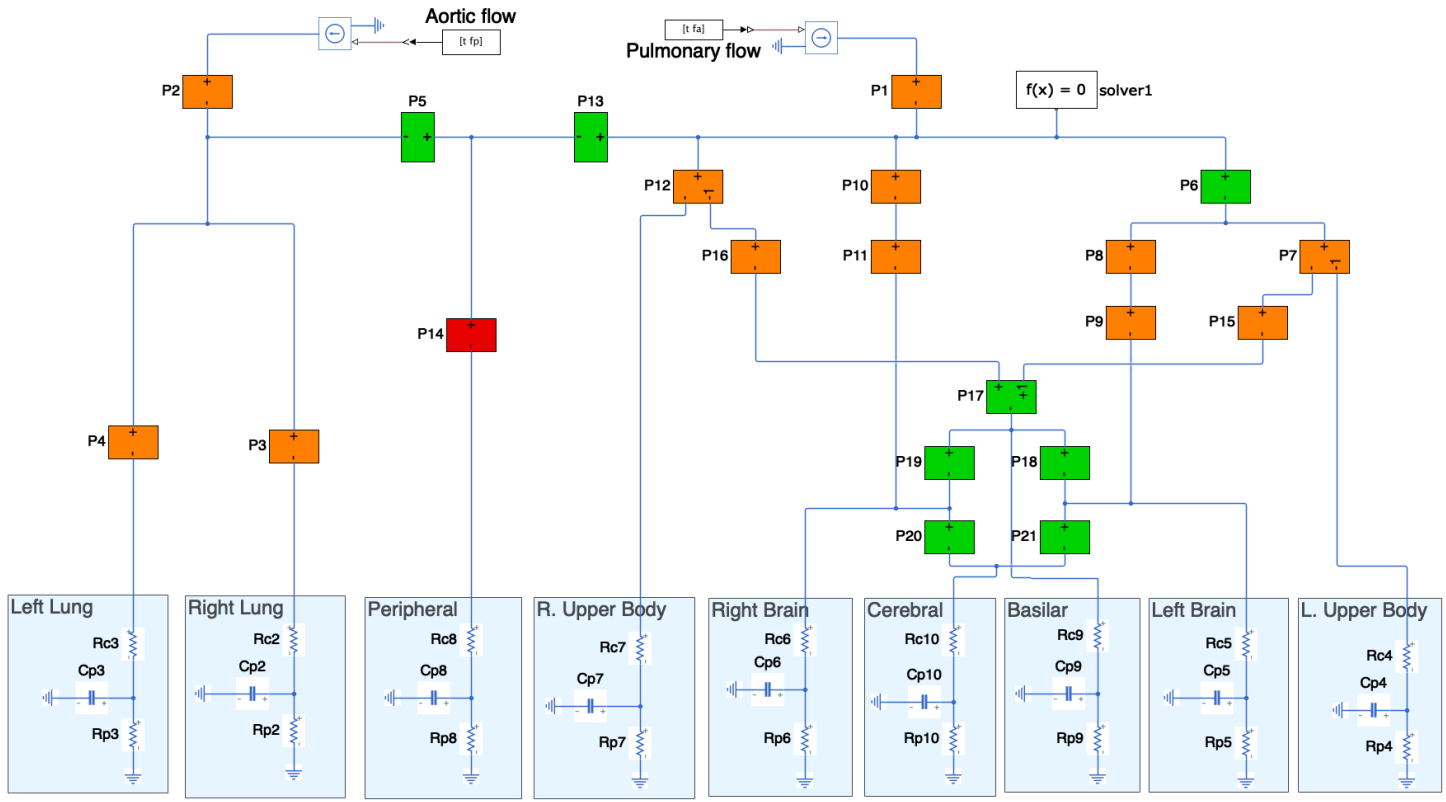


**Figure 4.3:** Simscape model for a simplify cardiovascular system. The rectangle boxes are subsystems, where each box represents a blood vessel. The color of the box denotes the number of compartments in each subsystem, where green is one, orange is five, and red is ten. The number on the box corresponds to the numerical number of a vessel in the anatomical configuration (see figure 4.2).

### 4.2.1 The Input

In this model, the current is choose as an input instead of the pressure. This is because flow measurements are more available. Pressure measurements at various locations are difficult to obtain and do not have good accuracy, compared to flow which can easily be accessed with ultrasound. The input flow or current in the simulation can either be generated by mathematical functions or acquired data from experiments. This data is stored in Matlab and then extracted by Simscape when the program is running. To convert velocity data from a blood vessel into flow rate, the velocity data need to be scaled by the cross-sectional area of the vessel. This is given by

$$\text{flow} = \text{velocity} \cdot \pi r^2 \quad , \tag{4.1}$$

where $r$ is the radius of the vessel. Besides, the flow can also be scaled by a factor of 0.5 if the velocity profile is assumed to be fully developed. This factor is needed because only the maximum velocity is given by Doppler measurements while the velocity in a blood vessel varies from its center to the vessel wall.

### 4.2.2 The Central Arteries

Every central artery in the model is substituted by a subsystem containing either one (represented by the green boxes), five (orange) or ten (red) compartments as shown in figure 4.4.

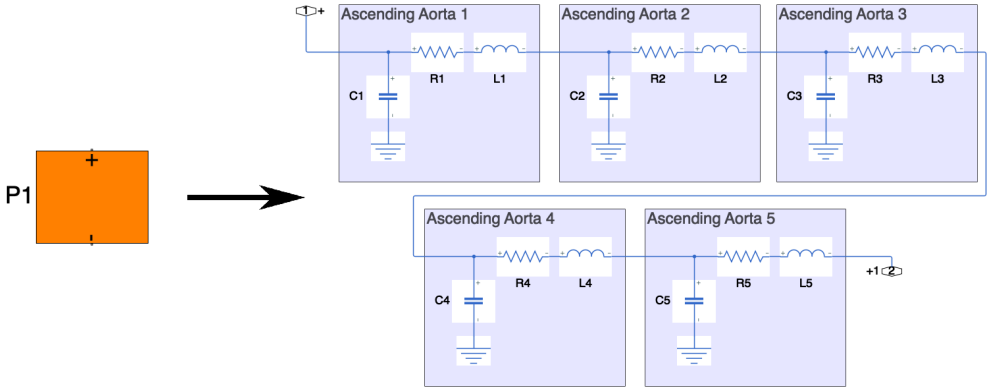


**Figure 4.4:** Each subsystem which represents a vessel can contain from one to ten compartments where every compartment is a combination of three electric elements ($R$,$L$ and $C$).

Each compartment in these subsystems consists of three lumped elements, a resistor and an inductor coupled in serial and a capacitor in parallel. So, instead of one single compartment for each blood vessel, the vessel is divided into smaller fractions, where each fraction is represented by a single compartment. There are two main reasons for this layout. The first one is to reduce the transient oscillation caused by inductors and

capacitors in some specific configurations (see section 2.4.7). By dividing into sections, the change is more distributed over space, and the values of each parameter also reduced, which make the transient oscillation less important. The other main reason is to increase the spatial distribution. Figure 4.5 shows the difference in flow waveforms between a single compartment and a multiple compartments representation of the main pulmonary artery.

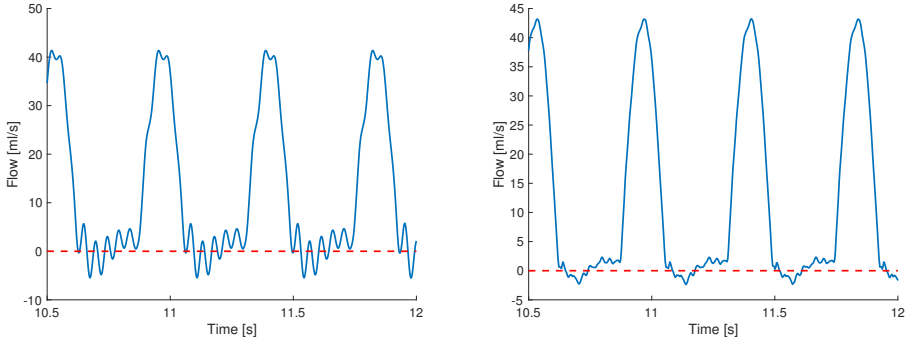


**(a)** One compartment for each vessel **(b)** Multiple compartment for each vessel

**Figure 4.5:** Comparison in flow waveforms between a single compartment (a) and multiple compartments (b) representation of the main pulmonary artery.

For each section of the vessel, the value of each parameter is calculated from relations described in section 2.4.6 using the physiological data from table 4.1. The compartments are evenly distributed along the length of the vessels. In addition to fractionating each blood vessel, the calculated value of each parameter (RLC) based on the collected data on section is also scaled with some factor.

### 4.2.3 The Vascular Beds

All vascular beds in the anatomical model are replaced by a compartment of three elements: a characteristic impedance $R_c$ that represents the resistance from the feeding artery to the point of interest. $Rp$ and $Cp$ account for the peripheral resistance and compliance. These block can either represent a small vascular bed or a whole body part. The values for these parameters are not given and are parameterized such that the pressure and flow distribution lies in a desirable range.

Chapter 5

# Results

This chapter covers all inputs and results from simulations and measurements. It is written out such that results from various aspects of the model are shown to validate the potentials and weakness of the implemented model. Clinical measurements from infants will also be included to compare and assess the capability of the model to correctly describe the waveform observed in both pressure and flow at various location. All assumptions and estimations are also listed so that all main factors that affect the results can be reflected on. The physiological model is illustrated in figure 4.2, and its equivalent electric model is shown in figure 4.3. The same model is used in all simulations with various boundary condition and state of the parameters. Simulation parameters are estimated based on the collected data in table 4.1 and the chosen configuration for each vessel.

## 5.1 The General Condition

All simulations in this sections are based on general conditions, meaning that the boundary conditions and parameter states are estimated from healthy neonatal, where the ductus arteriosus is not closed yet (1-2 days after birth). The use of general condition is for the practical purpose, since a more considerable amount of data is available for healthy infants compared to unhealthy ones. These data show the physical change dynamically as a function of time, which this study is trying to recreate.

The simulation flow inputs for the general condition are created with a mathematical function, a modified sinus function in this case. Figure 5.1 shown the input flows implemented by Matlab. This is generated with Matlab script A.1.

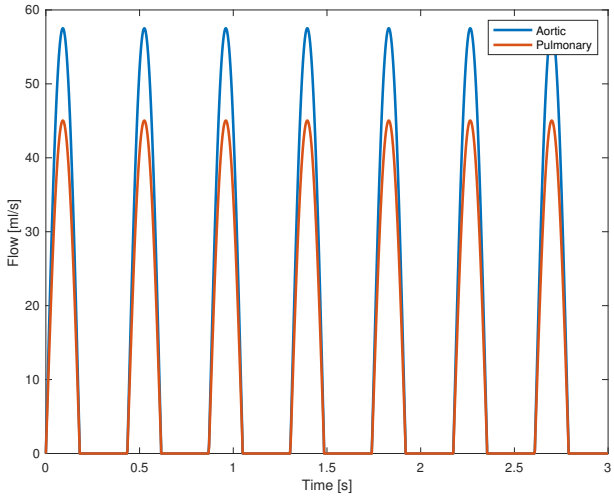


**Figure 5.1:** Input flows are generated by modified sinus function and represent the flows coming out of left ventricle (blue) and right ventricle (red).

The waveform, cycle periods, and amplitude are defined so that the stroke volume lies around 6.6 ml, assuming that the baby is about 3 kilogram. Table 5.1 lists all the initial and given values for a healthy newborn right after birth. The left and right ventricle stroke volume and heart rate are retrieved from the literature [3, 57], and the systole and diastole period are chosen arbitrarily.

**Table 5.1:** Physiological values for generation of model-based ventricle flow for neonates with PDA [3].

| Measurement | term neonate |
|---|---|
| Heart rate (beats/min) | 138 |
| Systole/diastole | 0.4/0.6 |
| LSV (ml) | 6.6 |
| RSV (ml) | 5.2 |

LSV, left ventricle stroke volume
RSV, right ventricle stroke volume.

To simulate flow in a full-term newborn right after birth, the gestational age is set to 38 weeks, the total body resistance and compliance are estimated such that the blood pressure is in a range between 24 and 59 mmHg [58]. The total resistance and compliance are distributed between different parts of the body, such that the amount of blood to every vascular bed or body part is reasonable. In general, changes in one part does not affect other parts significantly as long as their ratio is the same. Table 5.2 shows the applied total resistance and compliance in the systemic and pulmonary circulation. It also includes var-

ious ratios that define the amount of blood that goes to different body parts. These values, combined with the total resistance and compliance, are used to calculate the peripheral resistance ($R$) and compliance $C$ for each vascular bed. With peripheral resistances calculated, these values are then divided between $R_c$ and $R_p$. The ratios between $R_c$ and $R_p$ used in this study are arbitrary and might vary to adapt to a more specific condition or observed flow at a specific location.

**Table 5.2:** Estimated values and conditions for a model-based simulation for neonates.

| Systemic circulation | | | | |
|---|---|---|---|---|
| Vascular bed | Distribution ratio | R ($\mathrm{mmHg \cdot s/ml}$) | C (ml/mmHg) | $R_p/R$ |
| Cerebral vascular bed | 0.02 | 450 | 0.0030 | 0.9 |
| Basilar vascular bed | 0.02 | 450 | 0.0030 | 0.9 |
| Left brain | 0.05 | 180 | 0.0075 | 0.9 |
| Right brain | 0.05 | 180 | 0.0075 | 0.9 |
| Left upper body | 0.08 | 112.5 | 0.0120 | 0.9 |
| Right upper body | 0.08 | 112.5 | 0.0120 | 0.9 |
| Lower body | 0.07 | 12.9 | 0.1050 | 0.9 |
| Total | 1.00 | 9* | 0.15 | - |
| Pulmonary circulation | | | | |
| Left lungs | 0.50 | 8 | 0.08 | 0.8 |
| Right lungs | 0.50 | 8 | 0.08 | 0.8 |
| Total | 1.00 | 4* | 0.16 | - |

* The total resistance is calculated using the equation for a parallel circuit.

With the given set up, the outcome will still not be acceptable, where the pressure and flow waveforms differ significantly from the reference waveforms (see figure 3.3). To achieve more consistent results, and also a more realistic scenario, both the compliance and inductance in all central arteries are scaled down from calculated values described in section 4.2.2. Inductance is scale by a factor of 0.1 and compliance is scale by a factor of 0.5. To see how these scalings affect the overall pressure and flow, some simulations have been run with various scale factors both for compliance and inductance. The results are shown in figure 5.2

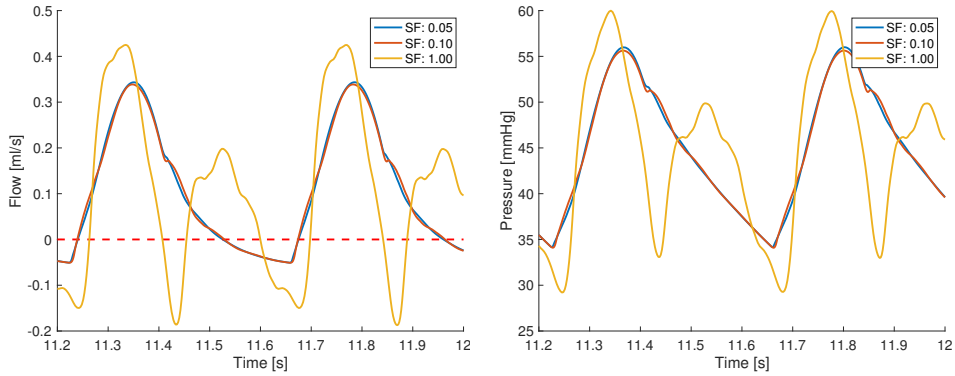


**(a)** Scaling $L$




**(b)** Scaling $L$

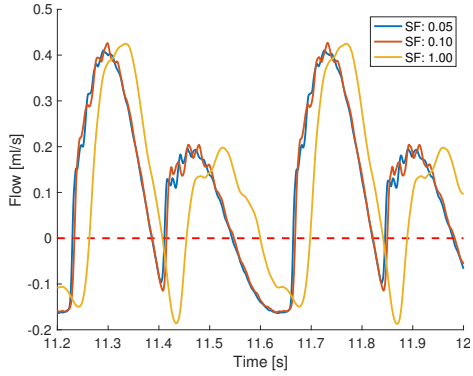


**(c)** Scaling $C$

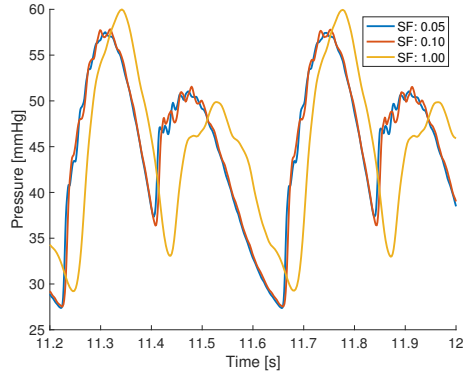


**(d)** Scaling $C$

**Figure 5.2:** Simulated pressure and flow waveforms for cerebral artery with various scale factor (SF) for inductance $L$ (a and b) and compliance $C$ (c and d)

These results are not only relevant to asses the consequence of these scaling, but also essential in understanding the weight and gravity of these parameters. Figure 5.2 shows what happens to flow and pressure when scaling either $L$ (a and b) or $C$ (c and d) for all central arteries. Only one segment is shown, but a similar change occurs in other segments. The displayed results in figure 5.2 shows that scaling the inductance $L$ does not change the blood distribution considerably, but compress the waveform of the flow and pressure and remove strange oscillation in the result. On the other hand, scaling the compliance $C$ does not affect the outcomes of the waveforms significantly, but shifted the waveforms slightly along the time axis.

Another important aspect of the simulations is that only the last part of the generated waveforms is used as the ending result both for displaying and analyzing. This is because the program takes some time to reach a steady state, and due to the instability, each simulation can only be run for 12 seconds. Hence the waveforms are assumed to have reached

a steady state before this time. Figure 5.3 shows how the flow and pressure developed into a steady state. The pressure takes most time to reach a steady state, but used under 4 seconds to reach a steady state. The steady state can be easily evaluated from the results, where if the pressure or flow keeps increasing or decreasing, then it is an indication that the simulation has not reached a steady state yet.

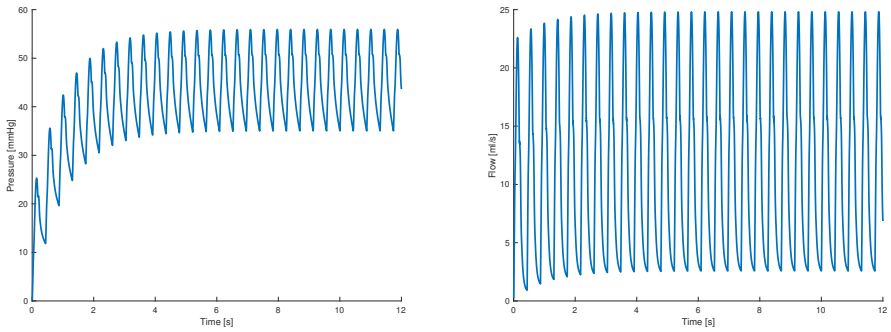


**(a)** Pressure development

**(b)** Flow development

**Figure 5.3:** Example of how waveforms develop into steady state for both pressure and flow.

## 5.2 Simulation Correspondence

As a next step the available data from the literature on infants with PDA was considered in the model. The current state of the model represents a neonatal circulation, right after birth, where the ductus arteriosus is still open. The results are shown in figure 5.4, where the general Doppler data from the literature [7] and measured velocities from ascending aorta and cerebral artery for infants with PDA are displayed in the top and the corresponding model-based flows are displayed in the bottom. The model-based pressure and flow are read from the resistor in the middle compartment of each vessel, except for cerebral readings which are read from $R_c$ in the cerebral compartment. The correspondence between the model-based and measured flows can easily be observed for the given selection of locations.

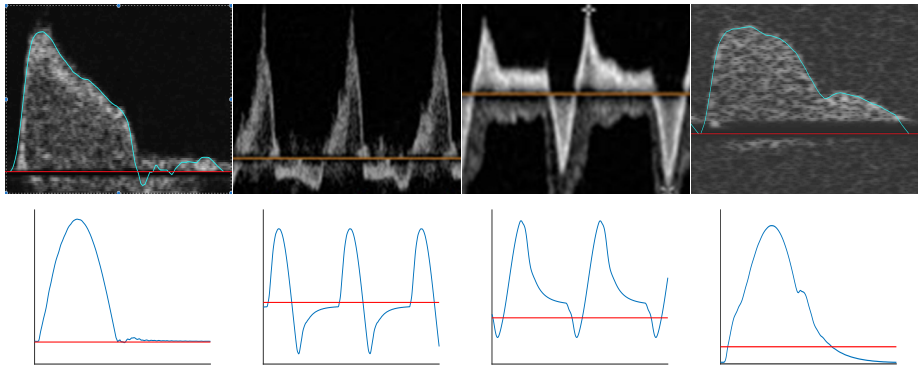

**(a)** Ascending Aorta **(b)** Descending Aorta **(c)** Ductus Arteriosus **(d)** Cerebral Artery

**Figure 5.4:** Measured flow (top) for infants with PDA and simulated flow (bottom) for newborn neonates with open DA. Doppler data is retrieved from Frontiers [7] and NeoDoppler data is measured experimental. The red line indicates the 0 flow value.

### 5.2.1 Closing of DA

In this section, more simulations have been carried out to observe how the implemented model is adapted to describe dynamic changes and how accurate it is when compared to real observation. To simulate the process of closing DA, several simulations have been run with various DA radius. The aim is to see how the blood distribution change and what effects the radius have on pressure and flow. The resulting pressures and flows for various sections of the body are shown in figure 5.5

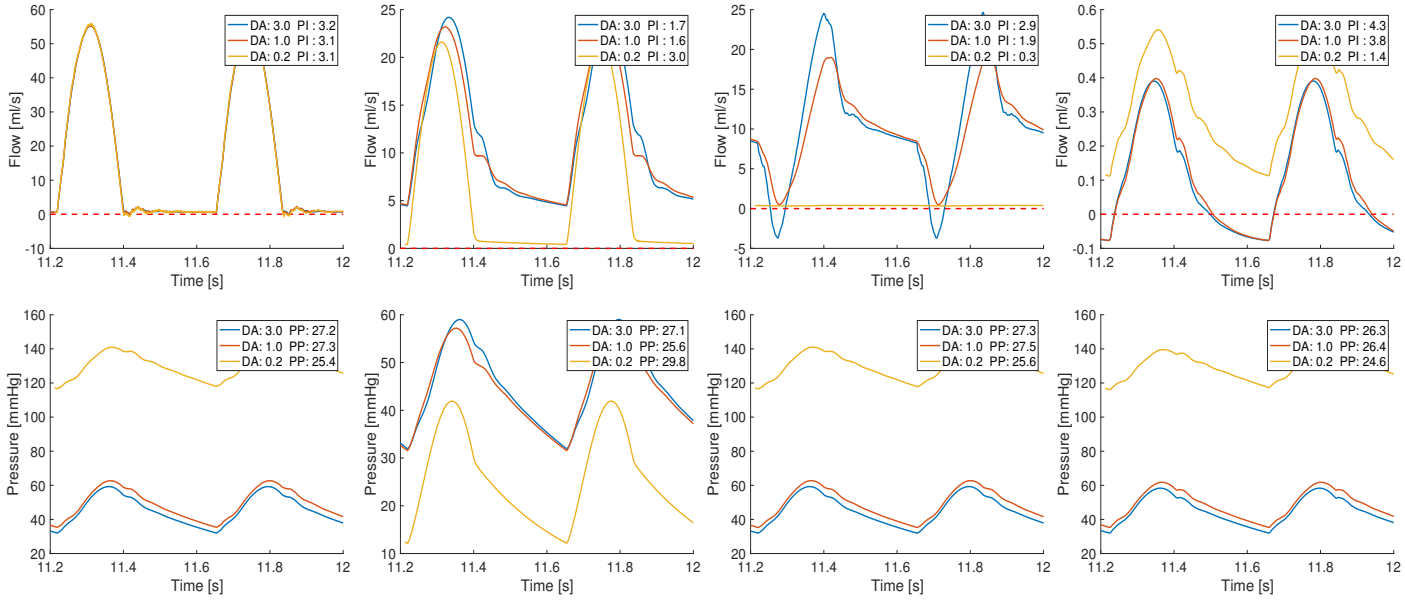


**(a)** Descending Aorta **(b)** Right lungs artery **(c)** Ductus Arterious **(d)** Cerebral Artery

**Figure 5.5:** Model-based waveforms for flow (top) and pressure (bottom) in a) descending aorta, b) right lung artery, c) ductus arteriosus, d) cerebral artery for different degrees of DA radius. The dash line indicates the zero flow limit. Pulsatility index (PI) and pulse pressure (PP) are calculated from the displayed waveforms.

On the systemic side, the flows (figure 5.5a and 5.5d) appear to be bidirectional when the DA radius is large and only push upward when the DA radius is reduced. When the DA radius becomes sufficiently small, one can observe that nearly no flow goes through the DA. As the DA radius decreases further, the pressure on the systemic side also increases rapidly. The resulting cerebral flow waveform is simplified, but it still has characteristics of the observed waveform from NeoDoppler both for open and close ductus (see figure 3.3). The PI values when the ductus is closed is also in the range of the observed values from NeoDoppler for healthy infants. On the pulmonary side, less flow is distributed to the lungs when the DA is closed and the PI increases since the peak flow is the same but the total amount is reduced.

The pressure waveforms and ranges are nearly the same for all segments and resemble a typical pressure waveform. The changes caused by closing the DA are different only between which side of the circulation one observes. On the pulmonary side, the pressure drops due to less blood that goes to the lung. These changes correspond well to the experimental data from the literature [59]. The pressure on systemic side acts entirely opposite to the pulmonary side. Since more blood goes to the rest of the body, the pressure increases as expected. However, the systolic pressure increases to a value around 150 mmHg, which is significantly higher than the normal value, around 70 mmHg [60]. To observe the change in pressure more continuously, more simulations have been run with a decreasing DA radius, where the pressure values and PI values are calculated and stored . These are shown in figure 5.6.

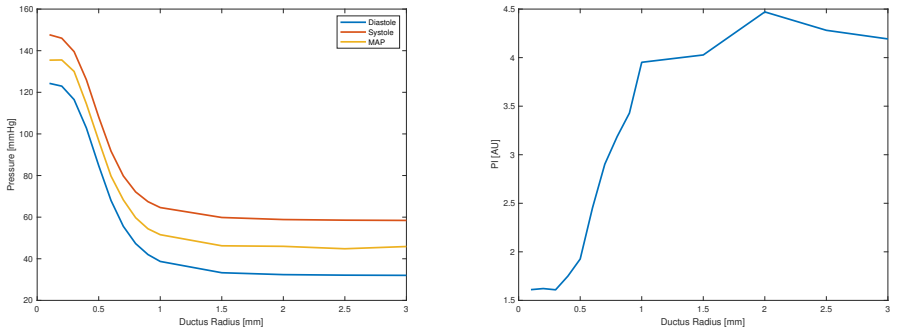


**(a)** Cerebral pressure

**(b)** Cerebral PI

**Figure 5.6:** Change in pressure values (systole, diastole and MAP) and pulsatility index (PI) in relation to a decreasing DA radius for cerebral artery.

### 5.2.2 Closing of DA with reduced Peripheral Resistance

Assuming that the peripheral resistance is reduced as a result of the increasing pressure caused by the closure of the DA, more simulations have been run with a decreasing DA radius and peripheral resistance. The choice of the total peripheral resistance on the sys-

temic side is based on how much the pressure increases as a function of the radius. In this study, the choice of total peripheral resistance is arbitrary and uses only qualitatively to observe additional changes. The ending result is displayed in figure 5.7. The pressure on the systemic side is still increasing, but reaches a more reasonable value around 65 mmHg.

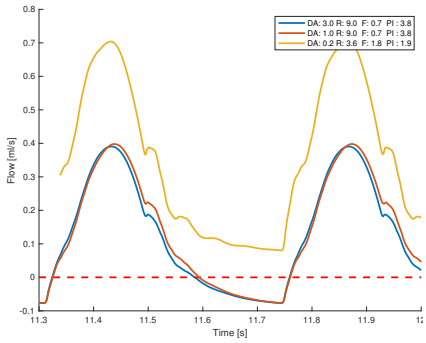


**(a)** Cerebral flow waveforms

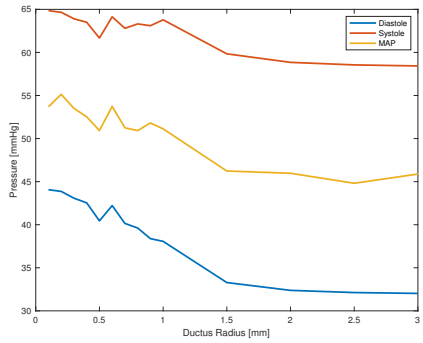


**(b)** Cerebral pressure

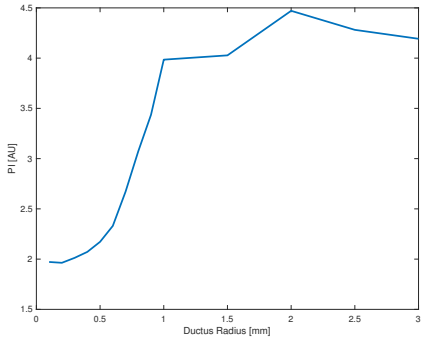


**(c)** Cerebral PI

**Figure 5.7:** Change in pressure values (systole, diastole, and MAP) and pulsatility index (PI) to a decreasing DA radius and peripheral resistance for cerebral artery. The cardiac output fraction (F) is calculated from the displayed waveform.

### 5.2.3 Heart Rate and Stroke Volume

In addition to the change in total peripheral resistance, the change in cardiac output also regulates the increased pressure. The heart rate and stroke are the main factors that control this regulation. The study in this section covers how the heart rate and cardiac output affect flow and pressure. Similar to previous simulations, the applied model and parameters are the same, but now with various heart rates and stroke volumes. The change of heart rate in these simulation does not affect the cardiac output, since the constructed input flows also changes dynamically as a function of the heart rate(A.1). Some studies have shown that

there is no clear correlation between cardiac output and heart rate [61], which corresponds well with the simulation setup. Figure 5.8 illustrates how various physiological parameters change according to the heart rate. These results show that as the heart rate increases, the pulse pressure and PI value decrease while the MAP remains constant.

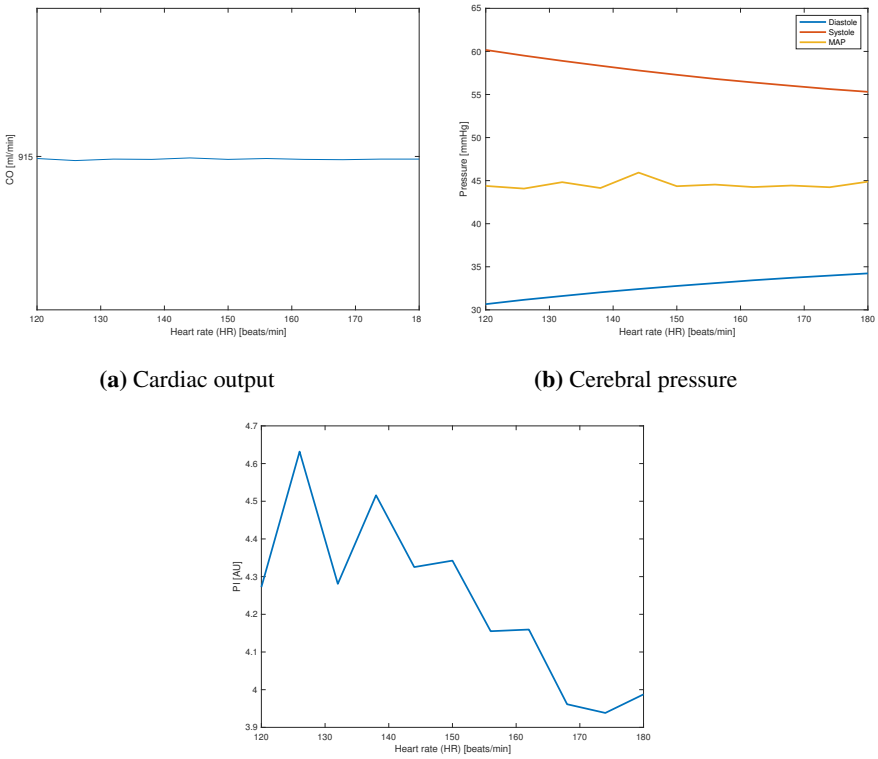


**(a)** Cardiac output

**(b)** Cerebral pressure

**(c)** Cerebral PI

**Figure 5.8:** Change in cardiac output, pressure values (systole, diastole, and MAP) and pulsatility index (PI) in relation to heart rate (HR).

While the heart rate (from simulations above) does not affect the cardiac output, the stroke volume, on the other hand, has a clear correlation to the cardiac output. To examine this correlation, several simulations are carried out with different stroke volume. An increase in the stroke volume can either mean that the output velocity is higher or a broader vessel opening. The outcome indicates a linear correlation between stroke volume and cardiac output, as shown in figure 5.9. The PI values do not appear to be affected by the stroke volume, whereas the pressure values increase proportional to the stroke volume.

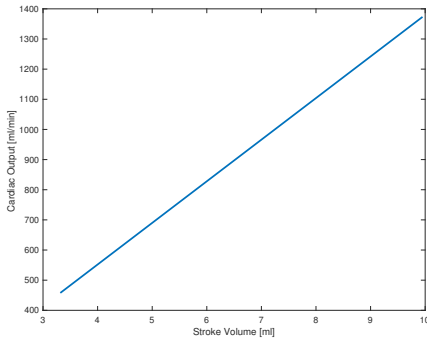


**(a)** Cardiac output

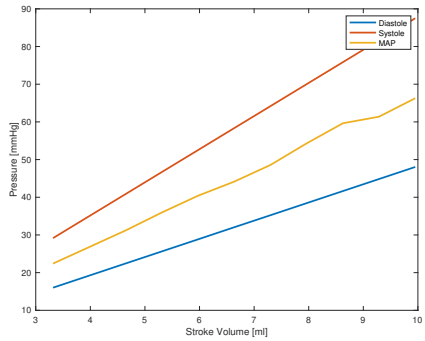


**(b)** Cerebral pressure

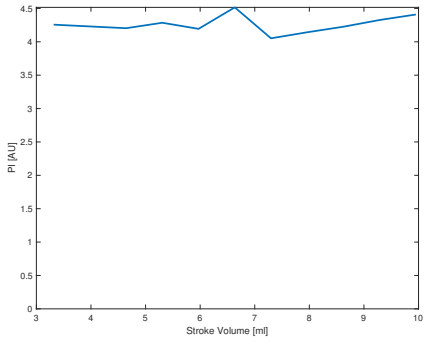


**(c)** Cerebral PI

**Figure 5.9:** Physiological change in cardiac output, pressure values (systole, diastole, and MAP) and pulsatility index (PI) in relation to stroke volume.

The settings above are simplified, where only one parameter is changed at a time. This approach might be inadequate in reality, where a change in heart rate or stroke often involved other factors such as the systole and the diastole periods. These again will typically affect the pulse pressure and PI value [62].

## 5.3 The Peripheral Compliance

The total peripheral or vascular compliance has so far been estimated such that the pulse pressure lies between 25 and 30 mmHg. This estimated value has been held constant under all previous simulations. To see how the total vascular compliance affects the overall results, several simulations have been run with different values of total vascular resistance, while all other parameters are kept constant. The results are shown in figure 5.10, where an increase in the total compliance seems to decrease the pulsatility of the pressure and flow.

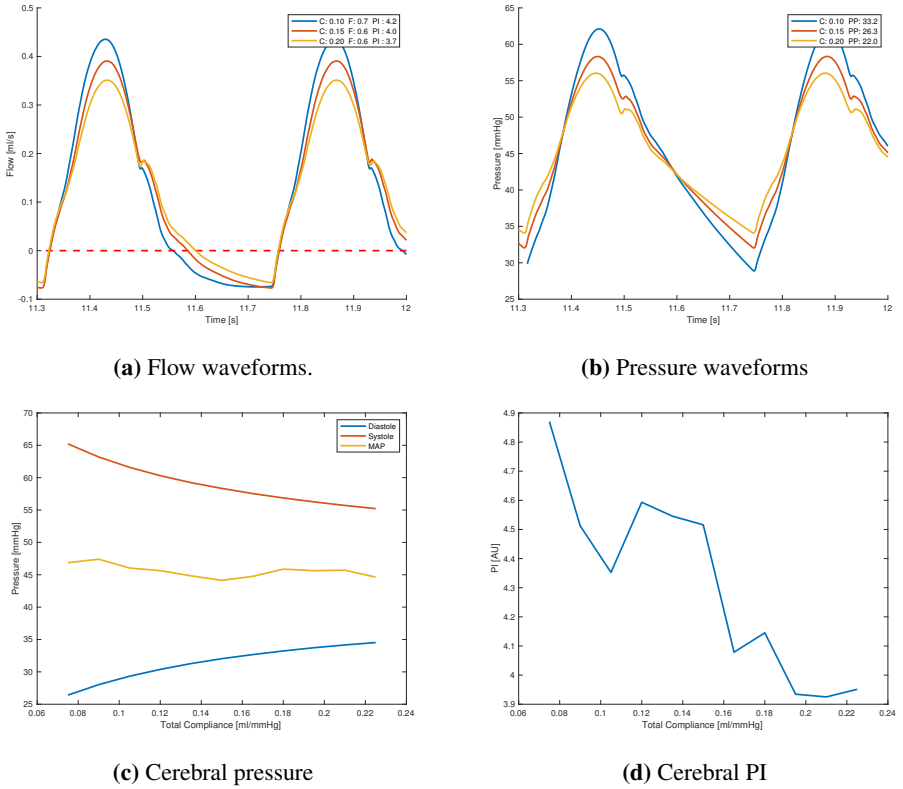


**(a)** Flow waveforms.

**(b)** Pressure waveforms

**(c)** Cerebral pressure

**(d)** Cerebral PI

**Figure 5.10:** Changes in a) cerebral flow waveforms, b) pressure waveform, c) pressure values, d) pulsatility index (PI) in relation to the total vascular compliance. The cardiac output fraction (F) is calculated from the displayed waveform.

## 5.4 The Clinical Condition

With only one set of measurements on an infant with PDA, this set is only used qualitatively to compare visually with the simulated results. From the appearance of these measurements, it is apparent that some of the data contain a considerable amount of systematic and random error. Hence, only parts of these recordings have been used to represent the input flows with some modifications. The experimental measurements also include the dimensions of some main arteries. These are listed in table 5.3, where the stroke volume and cardiac output in the right and left ventricle are estimated from the given dimension and their corresponding velocity data.

To generate a suitable simulation to match up with the measured results, some boundary conditions have been modified. These changes are based on the simulations runs on the background of this report and are listed in table 5.4. The input flows for this specific case are aortic and pulmonary flow collected from the patient. They are modified such that

**Table 5.3:** Patient specific cardiovascular values for a preterm infant with PDA.

| Measurement | Patient |
|---|---|
| Heart rate (beats/min) | 168 |
| AO radius (mm) | 2.5 |
| AO velocity peak (m/s) | 1.3 |
| LSV (ml) | 2.9 |
| PUL radius (mm) | 3 |
| PUL velocity peak (m/s) | 0.7 |
| RSV (ml) | 1.3 |
| DA radius (mm) | 1.25 |
| DA velocity peak (m/s) | 3.7 |

AO, Ascending aorta, LSV, Left ventricle stroke volume, PUL, Pulmonary artery, RSV, Right ventricle stroke volume, DA, Ductus arteriosus.

**Table 5.4:** Calibration of model-based physiological parameters for normal and preterm infants.

| Measurement | General state | Patient specific |
|---|---|---|
| Gestational age (GA) | 38 | 28 |
| Total system resistance ($\mathrm{mmHg \cdot s/ml}$) | 9 | 12 |
| Total pulmonary resistance($\mathrm{mmHg \cdot s/ml}$) | 4 | 6 |
| Total systemic compliance (ml/mmHg) | 0.15 | 0.1 |
| Total pulmonary compliance (ml/mmHg) | 0.16 | 0.1 |
| Ductus radius (mm) | 3 | 0.8 |

all reverse flow are removed and only one cycle is selected from data and repeats to create a sequence of cycles, as shown in figure 5.11. To convert the measured velocity to flow, the velocity of each vessel is scale by $0.5\pi r^2$, where $r$ is the radius of the corresponding vessel used in the simulation. Measured and simulated flow and pressure for some selected segments are shown in figure 5.12. The recorded flow waveforms are presented at the top, while the model-based results are displayed at the bottom.

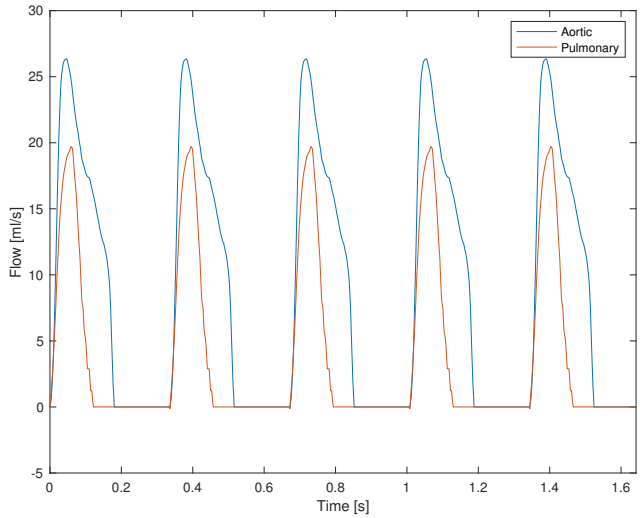


**Figure 5.11:** Modified measured flow as input flow for model-based simulation.

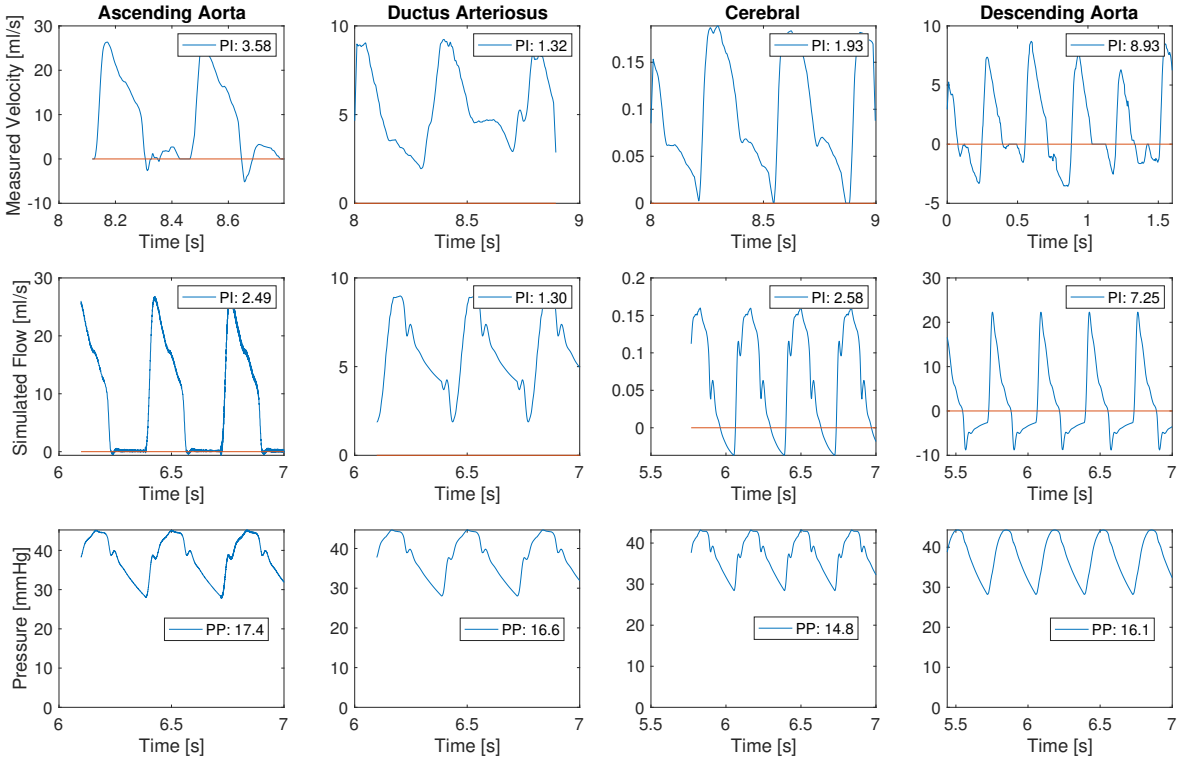


**Figure 5.12:** Simulated and measured flow for preterm infant with PDA. Doppler data is retrieved with standard Doppler techniques and cerebral blood flow is measured experimental with NeoDoppler. The red dash line indicates the 0 flow value.

The model-based and measured results from figure 5.12 shared some obvious similarities in the waveform, especially the flow through DA. The flow at cerebral artery is partly reversed in diastole, which gives a higher PI value compared to the one-directional NeoDoppler data. The rest of the PI values match well with the observed data when considering that only one cycle is used to calculate the PI value.

Chapter 6

# Discussion

In this chapter, the implemented model and results from simulations are discussed in detail. The main focus will be on the development of the models, tools, and techniques that are applied to simulate the system.

## 6.1 Anatomical Approach

The overall configuration of the implemented model was based on human anatomy, as described in section 4.2.2. The anatomical configuration was simplified only to consider the main arteries in the circulation system, including the Willis circle that supplies blood to the brain. Some major blood vessels have also been excluded from the model, including the left and right external carotid arteries which arise from the common carotid arteries and provide blood to the head and neck. These vessels were not included due to the increased complexity of the model and the limitations of the simulation tools. In the absence of the external carotid arteries, flows through the internal carotid arteries are expected to be higher and increased the flow to the left and right brain. Anatomically, this is not a correct representation. However, the focus of this model was to reconstruct the flow and its distribution to the cerebral arteries to compare with NeoDoppler data. Thus, the most important part of this work is to estimate the parameters that affect the blood distribution of the cerebral arteries.

## 6.2 Model Input

There were two types of inputs utilized in this work, generated and recorded flow. Generated input flows were based on the physiological conditions but generated with a mathematical function. For simplification, a sinus function was applied and modified such that

all negative values were set to zero. Generated inputs are simplified but still have some key features from the recorded data, including peak velocity, systole, and diastole periods and heart rate.

Recorded inputs were made from recorded velocity and converted to flow by multiplying with the cross-sectional area of the vessel where the input originates. This approach gives more realistic conditions compared to generated inputs. However, acquired signals often involve systematic and random errors, such as Brownian motion in the acoustic medium and thermal noise in the transducer and preamplifier [51]. Interference from neighboring blood vessels and veins will also contribute to the overall acquired signal. In addition, signal processing processes such as high-pass filtering also set low-velocity values to zero and create a rapid change in the estimated velocity. A rapid change or a stiff system will typically cause the simulation to slow down and sometimes collapse from its steady state. This is because the simulation is driven by differential equations.

## 6.3 Model Assumption

As a modification from previous models from the literature, some of the blood vessels were divided into small sections, where each of these sections was represented by a compartment of three electric elements (figure 4.2.2). This modification was mainly to remove the observed oscillation from simulation results. These oscillations are believed to originate from the configuration of resistance $R$, inductance $L$, and compliance $C$ or commonly known as the transient oscillation. By dividing each vessel into smaller sections, the length of each section is small and results in a smaller $C$ and $L$. The oscillation will disperse when the value of $C$ and $L$ is low enough due to a high resulted oscillation frequency that either is filtered out by the circuit (RLC-lowpass) or is no longer inside the observable range.

From the simulations in the background of this report, it was observed that the oscillation was reduced significantly with the current configuration compared to a configuration where every vessel was represented by only one compartment. The differences can be seen in figure 4.5. Another benefit of this modification is that it increases the spatial distribution, where more compartments were available to read the flow and pressure.

The disadvantage with this layout is that as the number of compartments or electric elements in the model increases, the error and instability of the system will also increase. Thus, the number of elements or compartments is limited for a given error.

Even with an increased number of compartments, the results still differ from the observed waveforms. To find out what affects the waveform, Several runs have been performed with different scaling factors for $R$, $L$, and $C$. Some of the results can be seen in figure 5.2. These results show that only by scaling down the $L$ values have a significant effect, where not only did it changed the shape of the waveforms, but also ending up with a similar waveform as observed in figure 3.3. The requirement of scaling to get reasonable waveforms indicates that some of these values might have been overestimated. These undesirable results might be a consequence of compressing a 3-dimensional system into a zero-dimensional model. The changes cannot happen over space but only at a single point.

Beside parameters in central arteries, lumped parameters in the peripheral compartments have also been estimated. These values were estimated arbitrarily to achieve flows and pressures within reasonable physiological limits.

## 6.4 Limitations of the Model and Simulation Tool

In general, a lumped parameters model for a cardiovascular system is developed from the main characteristics of the system and is sufficient to study the distribution of pressure, flow, and blood volume. The spatial distribution of the parameters can be included by adding more compartments, so-called multi-compartment models. For some simulation tool, such as Simscape, the dynamics of the real system can also be incorporated by adjusting the state of the parameters under run time.

However, the cardiovascular system is a complex system that involves many biological regulatory mechanisms and dynamic changes, where not everyone is fully understood. The simplified approach used in this work also limited the details of the system, where the implemented model was mainly used to evaluate the effects of the main components of the system (resistance, inductance, and compliance) for a given input. Physiological variables such as blood density, viscosity, and physiological dimensions of each vessel, were assumed to be constant under the simulation. Another important aspect is the technical limitations, where the simulations in this work can only be executed for a limited time interval with Simscape and then collapsed from its steady state. This instability was only observed in the current model, which contained 87 segments, distributed over all vessels and vasculatures. The increased number of segments in the model also increased the sampling frequency to conserve the upper limit of error. With high sampling frequency and rapid changes in the waveform, this combination is believed to increase the probability of instability. With a limited run-time, around 12 seconds for most of the cases, the generated waveforms were assumed to have reached a steady state before this time. This assumption is important because the pressure values and PI values were calculated from the last six cycles of the simulated results. This run-time limitation is sufficient for the runs done in this report, as shown in figure 5.3, where the program only used around 4 seconds to reach the steady state.

## 6.5 Simulation Correspondence

### 6.5.1 The General Condition

The similarities between the measured and simulated waveforms, as shown in figure 5.4, are observable, especially in the ductus arteriosus. The direction of the ductal shunt was bidirectional, but can also be right-to-left or left-to-right depending on the pressure difference between the systemic and pulmonary side. In the model, the direction of the shunt was determined by the total peripheral resistance of the systemic and pulmonary side of the circulation. The diastolic reverse flow in the descending aorta is also commonly observed

in infants with large PDA [63] and was reflected by the model result as well. From the displayed results, there was only the cerebral blood flow that differed considerably with a reverse flow at the end of the diastole period, whereas the measured flow was only one-directional and positive. How the flow in each segment depends on the DA radius can be seen in figure 5.5. The ductal closure was simulated by running simulations with various DA radius, while other variables and inputs were kept constant. This setup represents a system where the DA closes rapidly, and regulatory mechanisms have not yet occurred. Results from figure 5.5 shown that in most of the systemic segments, the diastolic reverse flow was reduced, and the amount of blood increased when reducing the DA radius. Further on, as the DA radius was lowered the amount of blood crossing the DA decreased rapidly. On the pressure side, the changes in each segment were similar to each other and differed only between the systemic where the pressure increased and the pulmonary side where the pressure decreased. All these changes in flow and pressure are as expected due to a redistribution of flow when ignoring possible biological responses.

What is typical in both the pressure and flow for every segment are that the changes happen rapidly at some specific radius. This transition range can be seen in figure 5.6 and revealed that the transition range for the DA radius was between 0.2 and 1 $\mathrm{mm}$.

### 6.5.2 Regulatory Effects

The resulting systolic pressure when the DA was closed without any regulation was about 150 mmHg. This value is too high for the neonates, where the normal value is about 70 mmHg [60]. This high pressure (hypertension) indicates that one or more regulatory mechanisms are involved in maintaining an optimal pressure value. To investigate some effects caused by regulatory mechanisms, various setups have been done with a focus on a specific parameter at a time, mainly input variables such as heart rate and stroke volume and boundary conditions such as total compliance and resistance. The results can be seen in figure 5.7, 5.8, 5.9, and 5.10 for cerebral blood flow. These setups were mainly to illustrate the possibility of the model to simulate dynamic changes and can be used to study the effect or impact from these variable. The results from these simulations show a diversity in the changes for each variable in relation to others. Furthermore, these results suggest that the cardiac output and total resistance define the ranges for SBP, DBP, and MAP, while the total compliance controls the pulsatility of the pressure and flow.

From the figures, one can also observe that both the MAP and PI values oscillate strangely. This oscillation can be explained from the way these values were calculated, which involved the mean values of a sequence. These sequences were defined dynamically under run time and did not have an integer number of cycle, and hence if the sequence is shifted a slightly, the outcome will change.

### 6.5.3 The Clinical Condition

With a set of Doppler data available for an infant with PDA, the model was personalized to fit these measured data. Table 5.4 lists all the changes in comparison to the general

condition, where the total body resistance was increased to maintain the systolic pressure around 45 mmHg. The pressure values in every segment are low since the cardiac output is much lower than the general state. The total compliance was also reduced, mainly to increase the pulse pressure and ending up around 16 mmHg for the given setup. The comparison between the recorded and simulated waveform is displayed in figure 5.12 and shows recognizable imitations in most of the segments. The only segment that stands out was the cerebral artery, which has a low reverse flow at the diastole and results in a higher PI value. This reverse flow indicates that flow in diastole might not zero as assumed, but a slightly positive as observed in the recorded waveform. Another possibility is that cerebral compliance was underestimated, where higher compliance will results in a slower decay in diastole. From the simulated results, it is also apparent that the waveforms contain some high-frequency oscillation, which can originate from the stiffness of the input. The results also included detail of the pressure, but since no pressure data were available, it is challenging to validate its accuracy. The pulse pressure seems to be small, but the patient condition was also critical, with high heart rate and low cardiac output.

Chapter 7

# Conclusion

In this thesis, a computational model has been developed to study the dynamics of pulsatile blood flow. The implemented model is a multi-compartment model and was based on the lumped parameters concept from previous models, initially developed for fetal circulation. This model was expanded to include the cerebral vascular network and modified by increasing the number of compartments to improve the spatial distribution.

To validate the model, each parameter was first adjusted to correlate to healthy neonates, and the results showed good correspondence with the observed flow and pressure waveforms from the literature. Then, the model was calibrated to emulate a patient-specific condition. In this case, the model was able to reconstruct waveforms that resembled the recorded waveforms. However, when adapting the model parameters for a PDA patient, a reverse flow was observed in the cerebral artery. In addition to the model limitations, the number of compartments in Simscape also has shown to limits the simulation run time and accuracy, where with the current setup, the simulation can only be run for 12 seconds. On the other hand, Simscape has been easy to use and useful in dynamic simulations and data analysis.

Regulatory mechanisms can also be included in the model by adding more components or increasing the functionality of each component. In this work, these regulations were not included due to limitations of the simulation tool and complexities of the overall effects.

## 7.1 Further Work

Several aspects of the model can be improved, depends on the desirable complexity and their objectives. As mention, modification can be done by adding more components or more functionalities to each component. To achieve better accuracy with the model developed in this report, the redistribution of flow caused by the left and right external carotid arteries need to be accounted for. These arteries are absent in the current model but can

be included by adding four more compartments, two for the blood vessels and two for the vascular networks associated with each vessel. The number of segments in each blood vessel can also be modified. These numbers have so far been chosen arbitrary, but can be reduced for some vessel to increased the simulation accuracy. Further, to make the model more complex, a heart and vein system can be added, this will give a more accurate overall picture and complete the circulation system. However, these modifications will limit the possibility to personalize the model to a specific patient, and the complexity of the heart will also be difficult to control and evaluate.

To get a better estimate of each parameter, more data can be collected, especially the physical properties of each blood vessel in healthy neonates and preterm infants. The relationship between these physical properties and the properties of the system should also be further investigated. This can be done by observing how the flow change as it moves from one vessel to another, using ultrasound imaging techniques. Besides observing spatial changes, recorded data is also important to validate the result and to estimate the boundary conditions.

# Bibliography


[1] Patricia Garcia-Canadilla, Paula A. Rudenick, Fatima Crispi, Monica Cruz-Lemini, Georgina Palau, Oscar Camara, Eduard Gratacos, and Bart H. Bijens. A computational model of the fetal circulation to quantify blood redistribution in intrauterine growth restriction. *PLOS Computational Biology*, 10(6):1–14, 06 2014.

[2] J. Alastruey, K.H. Parker, J. Peiró, S.M. Byrd, and S.J. Sherwin. Modelling the circle of willis to assess the effects of anatomical variations and occlusions on cerebral flows. *Journal of Biomechanics*, 40(8):1794 – 1805, 2007.

[3] Youtaro Agata, Satoshi Hiraishi, Koki Oguchi, Hitoshi Misawa, Yasunori Horiguchi, Nobuyuki Fujino, Kimio Yashiro, and Nobuhiro Shimada. Changes in left ventricular output from fetal to early neonatal life. *The Journal of Pediatrics*, 119(3):441 – 445, 1991.

[4] Wikimedia Commons. File:2916 fetal circulatory system-02.jpg — wikimedia commons, the free media repository, 2017. [Online; accessed 21-June-2019].

[5] OpenStax CNX. Blood Flow, Blood Pressure, and Resistance, 18 May. 2016. `https://cnx.org/contents/FPtK1zmh@8.25:A4QcTJ6a@3/Blood-Flow-Blood-Pressure-and-Resistance`. Accessed: 3 Des. 2018.

[6] Nico Westerhof, Jan-Willem Lankhaar, and Berend E. Westerhof. The arterial windkessel. *Medical & Biological Engineering & Computing*, 47(2):131–141, Feb 2009.

[7] Romaine Arlettaz. Echocardiographic evaluation of patent ductus arteriosus in preterm infants. *Frontiers in Pediatrics*, 5:147, 2017.

[8] Douglas J. Schneider and John W. Moore. Patent ductus arteriosus. *Circulation*, 114(17):1873–1882, 2006.

[9] James E. Dice and Jatinder Bhatia. Patent ductus arteriosus: an overview. *The journal of pediatric pharmacology and therapeutics : JPPT : the official journal of PPAG*, 12(3):138–146, 2007. 23055849[pmid].

[10] Stephanie Fuller and Peter J. Gruber. *Patent Ductus Arteriosus*, pages 283–288. Springer New York, New York, NY, 2011.

[11] Omar M. Khalid and Jacquelyn Busse. *Patent Ductus Arteriosus*, pages 113–121. Springer US, Boston, MA, 2011.

[12] E. R. Hermes-DeSantis and R. I. Clyman. Patent ductus arteriosus: pathophysiology and management. *Journal Of Perinatology*, 26:S14 EP –, Apr 2006. Original Article.

[13] Mair Zamir. *Hemo-Dynamics*. Springer International Publishing, Cham, 2016.

[14] Karaja T. Kokalari, I. and M. Guerrisi. Review on lumped parameter method for modeling the blood flow in systemic arteries. *Journal of Biomedical Science and Engineering*, 6(1):92–99, 2013.

[15] Tai-Wei Wu, Timur Azhibekov, and Istvan Seri. Transitional hemodynamics in preterm neonates: Clinical relevance. *Pediatrics Neonatology*, 57(1):7 – 18, 2016.

[16] Alex Tran. Modelling and monitoring bloodflow in premature infants with open ductus asteriosus using ultrasound Doppler technique. Master's thesis, Norwegian University of Science and Technology, NTNU, 2018.

[17] Anna Karoline Wisløff. Modeling of Peripheral Resistance in the Microvasculature for Diabetic Patients with Ultrasound Doppler Technique. Master's thesis, Norwegian University of Science and Technology, NTNU, 2018.

[18] Anders Hagen Jarmund. Cerebral Hemodynamics in Normal Neonates During Tilt: Computer Modelling and Experiments. Master's thesis, Norwegian University of Science and Technology, NTNU, 2019.

[19] Mehmet B. Yigit, William J. Kowalski, David J.R. Hutchon, and Kerem Pekkan. Transition from fetal to neonatal circulation: Modeling the effect of umbilical cord clamping. *Journal of Biomechanics*, 48(9):1662 – 1670, 2015. Reproductive Biomechanics.

[20] Sarah U. Morton and Dara Brodsky. Fetal physiology and the transition to extrauterine life. *Clinics in Perinatology*, 43(3):395 – 407, 2016. Birth Asphyxia.

[21] Camilla Lundberg, Pål Øian, and Claus Klingenberg. Umbilical cord clamping at birth–practice in norwegian maternity wards (in norwegian). *Tidsskrift for den Norske laegeforening : tidsskrift for praktisk medicin, ny raekke*, 133:2369–2372, 11 2013.

[22] Maryam Moradian. *Fetal Circulation*, pages 13–17. Springer London, London, 2014.

[23] Anthony J. Weinhaus. *Anatomy of the Human Heart*, pages 61–88. Springer International Publishing, Cham, 2015.

[24] David Hutchon. The normal range of heart rate at birth in a healthy term neonate: A critical review of the evidence. *Current Pediatric Research*, 20:7 –10, 02 2016.

[25] Salim Harris, Teuku Reyhan, Yetty Ramli, Joedo Prihartono, and Mohammad Kurniawan. Middle cerebral artery pulsatility index as predictor of cognitive impairment in hypertensive patients. *Frontiers in Neurology*, 9:538, 2018.

[26] Encyclopædia Britannica Britannica Academic. Artery, 14 Jan. 2016. `https://www.britannica.com/science/artery`. Accessed: 1 Des. 2018.

[27] Luis A. Martinez-Lemus. The dynamic structure of arterioles. *Basic Clin Pharmacol Toxicol*, 110(1):5–11, Jan 2012. PMC4435689[pmcid].

[28] Jean-Pierre Barral and Alain Croibier. 1 - general organization of the cardiovascular system. In Jean-Pierre Barral and Alain Croibier, editors, *Visceral Vascular Manipulations*, pages 3 – 26. Churchill Livingstone, Oxford, 2011.

[29] Encyclopædia Britannica Britannica Academic. The Blood Vessels, 13 Jul. 2018. `https://www.britannica.com/science/human-cardiovascular-system/The-blood-vessels#ref84863`. Accessed: 3 Des. 2018.

[30] Jordan D. Miller, David F. Pegelow, Anthony J. Jacques, and Jerome A. Dempsey. Skeletal muscle pump versus respiratory muscle pump: modulation of venous return from the locomotor limb in humans. *The Journal of physiology*, 563(Pt 3):925–943, Mar 2005. 15649978[pmid].

[31] John K. J. Li. *Dynamics of the Vascular System : Series On Bioengineering Biomedical Engineering*. World Scientific Publishing Co Pte Ltd, https://ebookcentral.proquest.com/lib/ntnu/detail.action?docID=231547, 2004.

[32] Beate H. McGhee and Elizabeth J. Bridges. Monitoring arterial blood pressure: What you may not know. *Critical Care Nurse*, 22(2):60–79, 2002.

[33] W. Boron and E. Boulpaep. Arteries and veins. In *Medical Physiology*, chapter 9. Elsevier, 3 edition, may 2016.

[34] Terrie E. Inder and Joseph J. Volpe. Chapter 13 - pathophysiology: General principles. In Joseph J. Volpe, Terrie E. Inder, Basil T. Darras, Linda S. de Vries, Adré J. du Plessis, Jeffrey J. Neil, and Jeffrey M. Perlman, editors, *Volpe's Neurology of the Newborn (Sixth Edition)*, pages 325 – 388.e26. Elsevier, sixth edition edition, 2018.

[35] Mair Zamir. *Mathematical Description of Fluid Flow*, pages 13–41. Springer International Publishing, Cham, 2016.

[36] William L. Hosch. Navier-stokes equation, August 2018.

[37] Encyclopædia Britannica Britannica Academic. Reynolds number, 25 Sep. 2017. `https://academic.eb.com/levels/collegiate/article/Reynolds-number/63389`. Accessed: 15 Nov. 2018.

[38] J.D. Jackson and Brian Launder. Osborne reynolds and the publication of his papers on turbulent flow. *Annual Review of Fluid Mechanics*, 39:19–35, 12 2006.

[39] Timothy W. Secomb. Hemodynamics. *Compr Physiol*, 6(2):975–1003, Mar 2016. 27065172[pmid].

[40] Patricia O'Brien and Audrey C. Marshall. Coarctation of the aorta. *Circulation*, 131(9):e363–e365, 2015.

[41] Mair Zamir. *Steady Flow in a Tube*, pages 43–80. Springer International Publishing, Cham, 2016.

[42] Mair Zamir. *Pulsatile Flow in an Elastic Tube*, pages 123–157. Springer International Publishing, Cham, 2016.

[43] Mair Zamir. *Dynamics of Pulsatile Blood Flow I*, pages 247–282. Springer International Publishing, Cham, 2016.

[44] H. E. Kallmann, R. E. Spencer, and C. P. Singer. Transient response. *Proceedings of the IRE*, 33(3):169–195, March 1945.

[45] Michael C. Faleski. Transient behavior of the driven rlc circuit. *American Journal of Physics - AMER J PHYS*, 74, 05 2006.

[46] Kiichi Sagawa, Reidar K. Lie, and Jochen Schaefer. Translation of otto frank's paper “die grundform des arteriellen pulses” zeitschrift für biologie 37: 483–526 (1899). *Journal of Molecular and Cellular Cardiology*, 22(3):253–254, Mar 1990.

[47] N Westerhof, G Elzinga, and P Sipkema. An artificial arterial system for pumping hearts. *Journal of Applied Physiology*, 31(5):776–781, 1971. PMID: 5117196.

[48] N. Stergiopulos, J. J. Meister, and N. Westerhof. Simple and accurate way for estimating total and segmental arterial compliance: The pulse pressure method. *Annals of Biomedical Engineering*, 22(4):392–397, Jul 1994.

[49] Kamran Hassani, Mahdi Navidbakhsh, and Mostafa Rostami. Simulation of cardiovascular system using equivalent electronic system. *Biomedical papers of the Medical Faculty of the University Palacký, Olomouc, Czechoslovakia*, 150:105–12, 08 2006.

[50] Omid Ghasemalizadeh, Mohammad Reza Mirzaee, B Firoozabadi, and Kamran Hassani. Exact modeling of cardiovascular system using lumped method. pages 408–417, 01 2008.

[51] H. Torp and L. Løvstakken. Doppler ultrasound. In *Comprehensive biomedical physics*, volume 2, chapter 14, page 343 – 360. Elsevier, (a. brahme, ed.) edition, 2014.

[52] H. Torp and B. A. Angelsen. Principles of medical ultrasound imaging and measurements. In *Ultrasound imaging - Waves, Signals and Signal processing in Medical Ultrasonics*, volume 1, chapter 1. Emantec AS, (a. brahme, ed.) edition, 2000.

[53] The MathWorks. Simulink. https://se.mathworks.com/products/simulink.html. Accessed: 3 Des. 2018.

[54] Patricia Garcia-Canadilla, Paula Rudenick, Fatima Crispi, Monica Cruz-Lemini, Georgina Palau, Eduard Gratacos, and Bart H. Bijnens. Understanding prenatal brain sparing by flow redistribution based on a lumped model of the fetal circulation. In Sébastien Ourselin, Daniel Rueckert, and Nicolas Smith, editors, *Functional Imaging and Modeling of the Heart*, pages 123–131, Berlin, Heidelberg, 2013. Springer Berlin Heidelberg.

[55] D G Mitchell, D A Merton, P J Mirsky, and L Needleman. Circle of willis in newborns: color doppler imaging of 53 healthy full-term infants. *Radiology*, 172(1):201–205, 1989.

[56] Otwin Linderkamp. Blood viscosity of the neonate. *NeoReviews*, 5(10):e406–e416, 2004.

[57] S J Clark, C W Yoxall, and N V Subhedar. Measurement of right ventricular volume in healthy term and preterm neonates. *Archives of Disease in Childhood - Fetal and Neonatal Edition*, 87(2):F89–F93, 2002.

[58] Thomas Hegyi, Mary Terese Carbone, Mujahid Anwar, Barbara Ostfeld, Mark Hiatt, Anne Koons, Jennifer Pinto-Martin, and Nigel Paneth. Blood pressure ranges in premature infants. i. the first hours of life. *The Journal of Pediatrics*, 124(4):627 – 633, 1994.

[59] Chunmiao Kang, Enfa Zhao, Yinghua Zhou, Huayun Zhao, Yunyao Liu, Ningning Gao, Xiaoxin Huang, and Baomin Liu. Dynamic changes of pulmonary arterial pressure and ductus arteriosus in human newborns from birth to 72 hours of age. *Medicine*, 95(3):e2599–e2599, Jan 2016. 26817918[pmid].

[60] K.L. Tan. Blood pressure in full-term healthy neonates. *Clinical Pediatrics*, 26(1):21–24, 1987. PMID: 3791834.

[61] Per Winberg and Ulf Ergander. Relationship between heart rate, left ventricular output, and stroke volume in preterm infants during fluctuations in heart rate. *Pediatric Research*, 31(2):117–120, 1992.

[62] V. Gemignani, E. Bianchini, F. Faita, M. Giannoni, E. Pasanisi, E. Picano, and T. Bombardini. Assessment of cardiologic systole and diastole duration in exercise stress tests with a transcutaneous accelerometer sensor. In *2008 Computers in Cardiology*, pages 153–156, Sep. 2008.

[63] Kyung Min Kim, Hyo Sup Kim, Ji Hong Yoon, Eun-Jung Lee, Sook Kyung Yum, Cheong-Jun Moon, Young-Ah Youn, Yoo Jin Kwun, Jae Young Lee, and In-Kyung Sung. Descending aorta blood flow characteristics before the development of necrotizing enterocolitis in preterm neonates. *Neonatal Medicine*, 25:78–84, 05 2018.

Appendix A

# Matlab code

## A.1 Input flow script

```
time = linspace(0,1,1000);
core = 2*pi*time*1.2;
ratio = pi/(2*pi*1.2);                  % Time share of
    systole
cp = round(ratio/(time(2)-time(1)));  % Zeros intersection
    point
scaleFactor = 1.1;
values = sin(core)*pi*a1*a1*scaleFactor;
values2 = 0.7*sin(core)*pi*a2*a2*scaleFactor;
% a1 and a2 is the radius of aorta and main pulmonary
    artery

hr = 2.3;               % Heart rate
time = time/hr;         % Scale the time for one cycle
values(cp:end) = 0;     % Remove negative flow
values2(cp:end) = 0;
rep = 60;               % Number of cycle repeated
t = zeros(rep*length(time),1);
fa = zeros(rep*length(time),1);
fp = zeros(rep*length(time),1);
t(1:length(time)) = time;
fa(1:length(time))= values;
fp(1:length(time))= values2;

for i = 1:rep-1
```

```
23      t(length(time)*i+1:(i+1)*length(time)) = t(length(time)
            *i) + time;
24      fa(length(time)*i+1:(i+1)*length(time)) = values;
25      fp(length(time)*i+1:(i+1)*length(time)) = values2;
26  end
27
28  LSV = sum(values*(t(2)-t(1))); % Left ventricle stroke
        volume
29  LVO = LSV*hr*60;               % Left ventricle cardiac
        output
30
31  RSV = sum(values2*(t(2)-t(1)));% Right ventricle stroke
        volume
32  RVO = RSV*hr*60;               % Right ventricle cardiac
        output
```

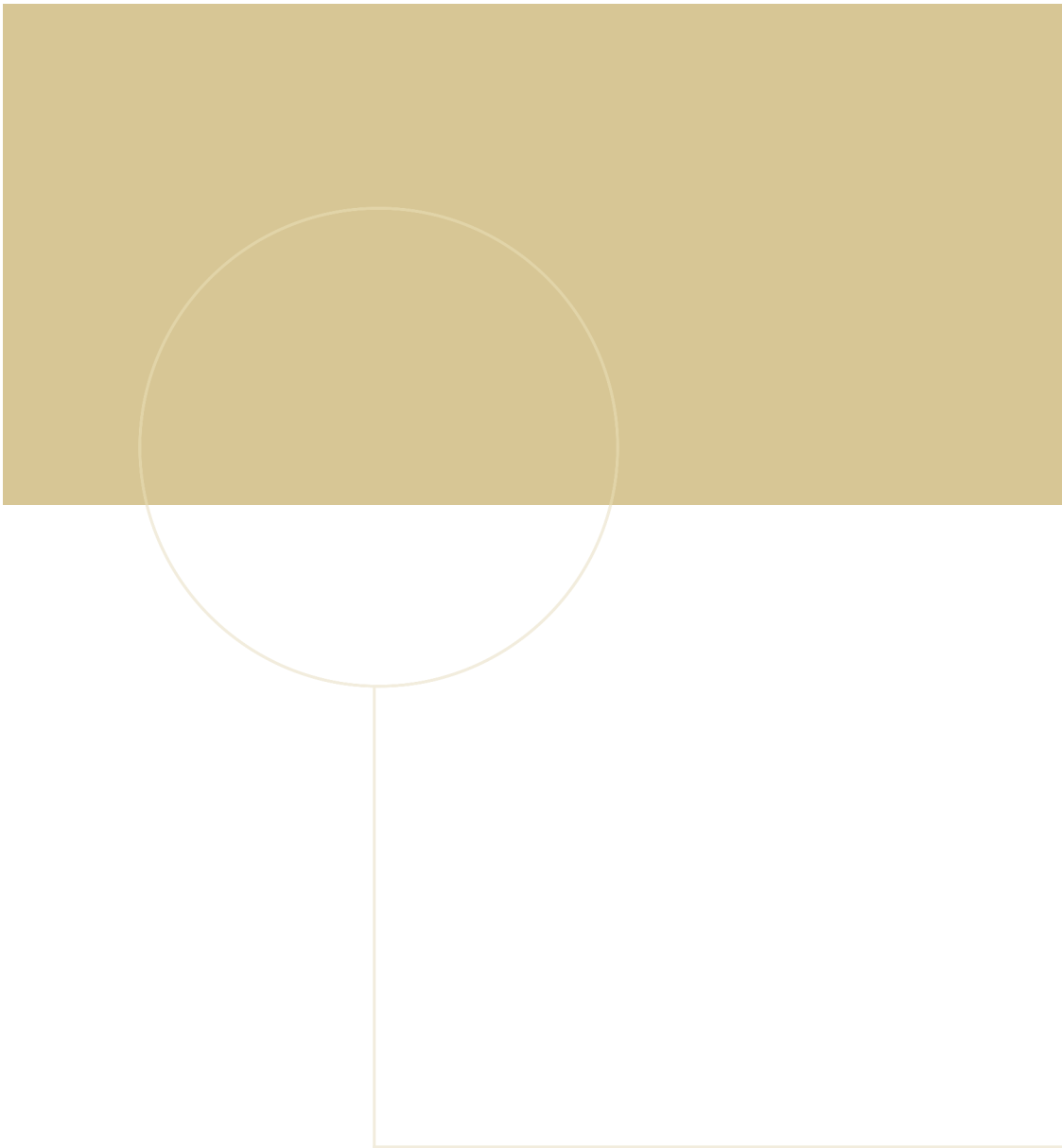

NTNU
Norwegian University of
Science and Technology